NACA

RESEARCH MEMORANDUM

for the

Air Materiel Command, U. S. Air Force

LONGITUDINAL STABILITY CHARACTERISTICS OF A $\frac{1}{40}$-SCALE MODEL OF

A PROPOSED CONFIGURATION OF THE XF-91 AIRPLANE MEASURED

BY THE WING-FLOW METHOD

By

Harold L. Crane and Arnold R. Beckhardt

Langley Aeronautical Laboratory
Langley Field, Va.

NATIONAL ADVISORY COMMITTEE
FOR AERONAUTICS
WASHINGTON

NATIONAL ADVISORY COMMITTEE FOR AERONAUTICS

RESEARCH MEMORANDUM

for the

Air Materiel Command, U. S. Air Force

LONGITUDINAL STABILITY CHARACTERISTICS OF A $\frac{1}{40}$-SCALE MODEL OF

A PROPOSED CONFIGURATION OF THE XF-91 AIRPLANE MEASURED

BY THE WING-FLOW METHOD

By Harold L. Crane and Arnold R. Beckhardt

SUMMARY

This report presents the results of an investigation in the tran-sonic speed range of the longitudinal stability characteristics of a proposed configuration for the Republic XF-91 airplane. The tests covered a Mach number range of 0.55 to 1.05 and a Reynolds number range from 400,000 to 1,375,000.

Lift, pitching-moment, and rolling-moment characteristics of the half model and the hinge moments on the all-moving tail were measured. The downwash factor $\partial\epsilon/\partial\alpha$ at the tail was determined from the pitching-moment data. A calculation of the elevator deflection and stick force required for trim was also made.

It was found that the variation of force and moment coefficients was linear through the test angle-of-attack range of -1° to 8° at any Mach number; that the stability increased markedly at Mach numbers above 0.85; that the effectiveness of the tail in producing pitching moments decreased about one-third with increasing Mach number; and that the value of the downwash factor, $\partial\epsilon/\partial\alpha$, at the tail decreased from about 0.35 at a Mach number of 0.85 to about zero at a Mach number near 0.95 and became slightly negative at higher Mach numbers. The calculated values of stick force per g and elevator deflection per g, assuming no aerodynamic balance, increased rapidly above a Mach number of 0.85.

INTRODUCTION

The NACA is conducting a series of investigations of the longi-
tudinal stability and control characteristics of several airplane con-
figurations. As part of this program a $\frac{1}{40}$-scale semispan model of a
prospective version of the Republic XF-91 airplane was tested in the
transonic speed range by the NACA wing-flow method. These tests were
requested by the Air Materiel Command, U. S. Air Force and the Republic
Aviation Corporation.

Tests were conducted to measure the lift, pitching moment, and
rolling moment of the half model with the tail on and off. Hinge moments
on the all-moving tail surface of the model were also measured. The
tests were run for an angle-of-attack range from approximately -1° to 8°
and for a tail incidence range from -6° to 3°. The Reynolds numbers for
the tests varied from 400,000 to 1,375,000. A Mach number range of 0.55
to 1.05 or slightly greater was covered.

SYMBOLS

The following symbols and coefficients are used in this report:

L   lift, pounds

M'   pitching moment (about 15 percent $\bar{c}$), foot-pounds

L'   rolling moment, foot-pounds

H   hinge moment (about 55 percent root chord of the tail), foot-
              pounds

C_L lift coefficient $\left(\frac{L}{qS}\right)$

C_m pitching-moment coefficient $\left(\frac{M'}{qS\bar{c}}\right)$

C_l rolling-moment coefficient $\left(\frac{L'}{qSb}\right)$

C_h hinge-moment coefficient $\left(\frac{H}{qS_t c_t}\right)$

$\dfrac{dC_m}{dC_L}$ rate of change of pitching-moment coefficient about 15 percent $\bar{c}$ with lift coefficient

C_{L_α} rate of change of lift coefficient with angle of attack

C_{m_α} rate of change of pitching-moment coefficient with angle of attack

C_{l_α} rate of change of rolling-moment coefficient with angle of attack

C_{h_α} rate of change of hinge-moment coefficient with angle of attack

$C_{L_{i_t}}$ rate of change of lift coefficient with tail incidence

$C_{m_{i_t}}$ rate of change of pitching-moment coefficient with tail incidence

$C_{l_{i_t}}$ rate of change of rolling-moment coefficient with tail incidence

$C_{h_{i_t}}$ rate of change of hinge-moment coefficient with tail incidence

q dynamic pressure, pounds per square foot $\left(\frac{1}{2}\rho V^2\right)$

S wing area, square feet

S_t tail area, square feet

c_T tip chord of wing, feet

c_R root chord of wing, feet

λ taper ratio $\left(\dfrac{c_T}{c_R}\right)$

$\bar{c}$ mean aerodynamic chord, feet $\left[\bar{c} = \frac{2}{3} c_R \left(\dfrac{1 + \lambda + \lambda^2}{1 + \lambda}\right)\right]$

c_t chord of tail, feet

b_e span of elevator along hinge line, feet

c_e elevator chord, feet

b wing span, feet

b_t span of horizontal tail

M model Mach number

M_A airplane Mach number

R Reynolds number

i_t tail incidence, degrees (measured in plane perpendicular to
               hinge line of model tail)

δ_e elevator deflection, degrees

$\dfrac{\partial i_t}{\partial \delta_e}$ relative elevator effectiveness

α model angle of attack, degrees

ϵ downwash angle, degrees (determined perpendicular to hinge
               line of model tail)

$\partial \epsilon / \partial \alpha$ downwash factor, the variation of downwash angle with angle
               of attack

K elevator gearing ratio, radians per foot

Full-scale values of lift, pitching moment, rolling moment, and
hinge moment may be found by using the coefficients presented herein
and the wing area and span of the complete airplane. The value of
rolling moment measured in these tests represents the bending moment
acting at the center line of the complete airplane.

DESCRIPTION OF APPARATUS

Photographs of the $\frac{1}{40}$-scale XF-91 wing-flow model and test apparatus are presented in figure 1. Sketches of the airplane and of the model showing principal dimensions are given in figures 2 and 3. Table I gives the principal geometric characteristics of the XF-91 model and the full-scale airplane. The model was made of brass and high-strength dural and steel alloys. The end plate, which was used as a reflection plane to simulate a full-span condition, was $\frac{1}{32}$ inch thick with feathered edges.

The model was mounted on the right wing of an F-51D airplane. A portion of the wing of this F-51 airplane has been modified to produce a contour with a low chordwise velocity gradient. This contour also gives a favorable location (behind the model) of the wing compression shock. Typical chordwise and vertical gradients of local velocity over a test panel are given in figure 4.

The center line of the model fuselage was bent to the curvature of the test panel to conform to the curvature of the flow along the model. The pivot axis of the model was located at 15 percent of the mean aerodynamic chord and the axis of rotation of the all-movable tail was at 55 percent of the tail root chord, perpendicular to the root chord, and in the plane of the tail.

The aerodynamic forces were measured with a strain-gage balance, and the model angles and tail deflections were measured with slide-wire potentiometers. A recording galvanometer made a continuous record of the angles, deflections, and aerodynamic forces. Airspeed, altitude, lateral and normal acceleration, and the free-air temperature were recorded with standard NACA instruments.

During flight the model was oscillated by an electric motor to vary the angle of attack. The model was oscillated through a range of about 8° at a rate of approximately one cycle per second. In flights where the tail was oscillated, an air-driven motor was used to oscillate the tail through a range of 10° at a rate of approximately one cycle per second. These rates of oscillation in terms of chord lengths of air flow over the model give a maximum rate of rotation of approximately 1° per 80 chord lengths which is believed to be sufficiently small to avoid any aerodynamic-lag effects.

The angle of flow across the wing was measured with a freely floating vane which was located 22 inches outboard of the model. A calibration of the difference in angle of flow between the model location and the vane location had been made before the model was installed.

TESTS

In all flights the wing was set at $0°$ incidence. Flights were made with three model configurations. The tail was fixed at approximately $0°$ and the model oscillated through an angle-of-attack range from $-1°$ to $8°$; the model was fixed at approximately $0°$ angle of attack with the tail oscillating from $-6°$ to $3°$; and with the tail off, the model was oscillated from $-1°$ to $8°$ angle of attack. The small angle-of-attack range over which data were obtained was a consequence of the large tail bearing block on the model which required a cut-out in the panel on which the test setup was mounted. Accidental interference between other parts of the test equipment also restricted the angle-of-attack range in some cases. These data were obtained during development of the test equipment; and since the configuration of the XF-91 was subject to change, it was not considered worth while to repeat the tests in order to obtain a larger angle-of-attack range.

During each flight runs were made at two different altitudes to extend the Reynolds number range. A "level-flight" run was made at an altitude of 5000 feet after a pull-out from a dive with the airplane speed gradually being reduced from 450 to 220 miles per hour. This run gave a model Mach number range from about 0.95 to 0.55 with a Reynolds number range from 1,325,000 to 880,000 based on the model mean aerodynamic chord. The "high dive" run was made in a $25°$ dive from an altitude of 28,000 feet. The dive was entered at an indicated airspeed of 220 miles per hour and the pull-out was made at an airplane Mach number of 0.73. The "high dive" runs gave a model Mach number range from 0.65 to 1.05 or slightly greater with Reynolds numbers from 460,000 to 790,000. The relations between Reynolds number and Mach number for the data presented herein are given in figure 5.

PRESENTATION OF RESULTS

A view of a sample record from the six-element galvanometer is presented in figure 6. The irregularities in the pitching-moment trace were introduced by the driving mechanism rather than by buffeting.

Typical plots of the wing-flow data as they were first worked up are presented in figure 7, one plot for each configuration. The force and moment coefficients were determined from the following expressions:

$$C_L = \frac{L}{qS}$$

$$C_l = \frac{L'}{qSb}$$

$$C_m = \frac{M'}{qS\bar{c}} \text{ (about 15 percent } \bar{c}\text{)}$$

$$C_h = \frac{H}{qS_t c_t} \text{ (about 55 percent root chord)}$$

The hysteresis in the lift data was due to electrical overdamping of the galvanometer element and not to any aerodynamic lag.

An estimation of the accuracy of the various measurements is presented in the following table. Possible errors in absolute values and in increments of the specified variable read from faired curves are presented. Errors are also given in terms of force and moment coefficients. Errors in the absolute values of the forces and moments measured on the strain-gage balance system may be caused by undetected zero shifts in the balance calibration, as well as by undetected changes in the slope of the calibration curve. These errors are therefore larger than the errors in the increments of the measured quantities during a given run or series of runs which are usually not affected by zero shifts. Errors in the lift data appear to be more serious than those in the other measured quantities. As previously noted, error may be introduced in measuring the slope of the lift curve by the hysteresis loop present in these data. In addition the angle of zero lift appears to vary in an unexplained manner in various runs. The pitching-moment data are subject to errors involved in fairing out the irregularities in the record line introduced by the driving mechanism. It should be noted that errors in coefficients vary inversely with dynamic pressure. The values presented for possible errors do not take into account the effects of the velocity gradient over the model.

Variable	Possible error		
	In absolute value	In increment	In coefficient (absolute value)[1]
Mach number M	±0.01	-----	-----
Dynamic pressure q, percent	±1.0	-----	-----
Angle of attack α, deg	±.4	±0.1	-----
Tail incidence i_t, deg	±.2	±.05	-----
Lift L, lb	±1.0	±.4	±0.06
Pitching moment M', in.-lb	±1.0	±.4	±.02
Rolling moment L', in.-lb	±1.0	±.4	±.01
Hinge moment H, in.-lb	±.1	±.05	±.02

[1]For minimum dynamic pressure, 36 inches of water.

The variation of lift and moment coefficients with angle of attack or tail incidence for the XF-91 half-model are presented in figure 8 for the tail-off case, in figure 9 for the tail-on and fixed configuration, and in figure 10 for the tail-oscillating case. The symbols used on these curves are for identification only and do not represent test points. The data are presented for increments of Mach number of 0.05 or 0.10 throughout the test range and for the two Reynolds number ranges.

The slopes C_{L_α}, C_{m_α}, C_{l_α}, and the stability parameter dC_m/dC_L are presented in figure 11 as a function of Mach number for the tail-off configuration and in figure 12 with the addition of C_{h_α} for the tail-on and fixed configuration. Figure 13 gives the slopes $C_{L_{i_t}}$, $C_{m_{i_t}}$, $C_{l_{i_t}}$, and $C_{h_{i_t}}$ as a function of Mach number for the tail-oscillating case. It should be noted that $C_{L_{i_t}}$ is the variation of the lift coefficient based on wing area with tail incidence.

The rate of change of downwash at the tail with angle of attack $\partial\epsilon/\partial\alpha$ at Mach numbers throughout the test range was determined by use of the pitching-moment data of figures 8, 9, and 10 to calculate the change in tail incidence required to maintain zero pitching moment due to the tail when some specified change in angle of attack was made. The variation of $\partial\epsilon/\partial\alpha$ with M is presented in figure 14.

DISCUSSION OF RESULTS

General

Examination of the data as a whole showed that the variation of all force and moment coefficients with angle of attack or tail incidence was linear through the test ranges of $-1°$ to $8°$ and $-6°$ to $3°$, respectively. The slopes of these curves changed gradually with Mach number. No complete loss or reversal of lift-producing effectiveness of the airfoil surfaces was discovered. Over the test range of Reynolds number, the effect of Reynolds number on the force and moment coefficients was rather large. Any large changes in the character of the variations of C_{L_α} and C_{l_α} with Mach number seemed to occur at a lower Mach number when the Reynolds number was increased. The angles of zero lift obtained from the lift data are inconsistent. The angles of zero rolling moment appear to indicate more reasonable angles of zero lift which are in agreement with low-speed wind-tunnel data.

Tail Off

The slope of the lift curve C_{L_α} measured from figure 8 and plotted on figure 11 was approximately 0.035 at M = 0.5 and tended to increase with Mach number. The maximum value of C_{L_α} was 0.045 at M = 0.8 from the higher Reynolds number data. At Mach numbers above 0.8, C_{L_α} fell off appreciably for the higher Reynolds number data but held constant at approximately 0.04 up to M = 1.1 for the low Reynolds number data. The lift-curve slope of 0.035 obtained at M = 0.5 was considerably lower than the value of 0.05 obtained in references 1 and 2 at low speeds. The tail-off angle of zero lift obtained from the rolling-moment data was about $-1°$ which was in agreement with reference 3.

The tests were made with a simulated center-of-gravity position at 15 percent mean aerodynamic chord. The XF-91 model was unstable with tail off at low Mach numbers. The variations of the longitudinal stability

parameters C_{m_α} and dC_m/dC_L with Mach number were small up
to $M = 0.85$ where the stability began to increase. The extreme aero-
dynamic-center locations with tail off were approximately 5 percent
mean aerodynamic chord at $M = 0.5$ and 35 percent at $M = 1.1$. Agree-
ment with low-speed tunnel data (reference 1), which gave a tail off
aerodynamic-center location of 10 percent mean aerodynamic chord, was
fairly good.

The variation with Mach number of the rate of change of rolling-
moment coefficient with angle of attack C_{l_α} was similar to that of
the lift-curve slope C_{L_α}. An outboard shift of the center of lift of
between 5 percent and 10 percent $\frac{b}{2}$ with increasing Mach number was
indicated.

Tail On and Fixed

Figure 12 shows that the slope of the lift curve was increased
approximately 10 percent by the tail surface. The variation of lift-
curve slope with Mach number and Reynolds number was similar to that
obtained with tail off.

Comparison of the variation of C_{m_α} and dC_m/dC_L with Mach number
in figures 11 and 12 indicates that the contribution of the tail to
longitudinal stability was approximately constant. The increment
of dC_m/dC_L due to the tail was approximately -0.2. The aerodynamic
center of the XF-91 model with the tail on was at approximately 25 percent
mean aerodynamic chord at $M = 0.55$ and at 60 percent mean aerodynamic
chord at $M = 1.05$. This fact indicates that there was a large increase
with Mach number in stick-fixed stability for maneuvers at constant speed.
Once again, agreement with the low-speed tunnel data (references 1 and 3),
which gave a tail-on aerodynamic center location of 26 to 28 percent mean
aerodynamic chord, was good. The missile data of reference 4 gave a
value of C_{m_α} of -0.02 with the center of gravity at 5 percent mean
aerodynamic chord at a Mach number of 1.0. For a lift-curve slope of
0.044 the aerodynamic center would be at 50 percent mean aerodynamic
chord compared to the value of 60 percent obtained from the wing-flow
tests.

The balance was equipped to measure hinge moments of the tail about
an axis at 55 percent of the root chord. The value of C_{h_α} was in the
neighborhood of -0.01 and increased considerably with increasing Mach
numbers above $M = 0.85$.

Tail Oscillating

The data of figures 10 and 13 indicate that the effectiveness of
the tail surface in terms of the increment of airplane lift coefficient
produced per degree change in incidence was subject to a gradual decrease
with increasing Mach number. Most of the decrease came above $M = 0.85$.
The average extreme values of $C_{L_{i_t}}$ were approximately 0.007 at $M = 0.6$
and 0.003 at $M = 1.05$. Reference 3 indicates that the low-speed value
of $C_{L_{i_t}}$ is 0.01 or slightly less.

The variation with Mach number of the rate of change of pitching-
moment coefficient with tail incidence was similar to the variation
of $C_{L_{i_t}}$. Above $M = 0.9$ the value of $C_{m_{i_t}}$ decreased approximately
one-third. Reference 3 gives a low speed value of $C_{m_{i_t}}$ of -0.013 which
is very close to the value of -0.0125 obtained at $M = 0.55$ in the present
tests.

Downwash

The tail-off and tail-on pitching-moment data and the tail effec-
tiveness data have been used to determine tail settings at which the
tail produced no pitching moment and was therefore lined up with the
air stream. From this procedure it was possible to determine the rate
of change of downwash angle at the tail with angle of attack. This
method of getting $\partial\epsilon/\partial\alpha$ is subject to an accumulation of the errors
in each of the measured quantities used and errors from the graphical
process involved. Hence, it is expected that the values of $\partial\epsilon/\partial\alpha$ are
accurate to ±0.05. Figure 14 shows that the downwash tended to increase
with Mach number up to $M = 0.85$ and then to decrease until at a Mach
number of 0.94 and above a slight amount of upwash existed over the tail.
The values of downwash factor obtained at the lower Mach numbers ranged
from 0.27 to 0.35. The maximum value of $\partial\epsilon/\partial\alpha$ determined was 0.38
at $M = 0.85$ in the low Reynolds number run.

A calculation of the downwash factor was made from the data of
reference 3. These data gave excellent agreement with the data obtained
in these tests for the values of $\partial\epsilon/\partial\alpha$ at a Mach number of 0.65 and
for the high Reynolds number range. The tests of reference 3 were made
at a Reynolds number of 1,100,000.

The contribution of the tail to the longitudinal stability did not
vary appreciably with Mach number since the tail effectiveness $\left(C_{m_{i_t}}\right)$

decreased with increasing Mach number while the value of $\left(1 - \dfrac{\partial \epsilon}{\partial \alpha}\right)$ increased with increasing Mach number.

Calculation of Elevator Deflection And Stick Force for Trim

Calculations of elevator deflection required for trim and the control force which would be required with an elevator having no aerodynamic balance have been made for the full-scale XF-91 airplane. In addition to the wing-flow data for the higher Mach number range presented herein, data from references 4, 5, and 6 have been used in the calculations. The following airplane characteristics were used:

Wing area, square feet 320
Gross weight, pounds 25,000
Wing loading, pounds per square foot 78.1
Length of elevator, along hinge line, feet 17.34
Tail mean aerodynamic chord, parallel to air flow, feet 3.94
Elevator chord, percent of tail chord 30
Elevator chord, feet (perpendicular to hinge line) 0.98
Total stick travel, inches 18
Down-elevator deflection, degrees 25
Up-elevator deflection, degrees 35
Center-of-gravity position, percent $\bar{c}$ 15

An altitude of 20,000 feet was used in the calculations.

The expressions used for the calculations were

$$\delta_e = \frac{C_L \dfrac{dC_m}{dC_L}}{\left(C_{L_{i_t}} \dfrac{dC_m}{dC_L} - C_{m_{i_t}}\right)\dfrac{\partial i_t}{\partial \delta_e}} \tag{1}$$

$$F = KC_{h_\delta}\delta_e q b_e c_e^{\,2} \tag{2}$$

The values of dC_m/dC_L, $C_{L_{i_t}}$, and $C_{m_{i_t}}$ were obtained from the data presented herein for the higher Mach number range. Values of C_{h_δ} and $\partial i_t/\partial \delta_e$ for use in these calculations were obtained from reference 5. Figure 3 of reference 6 was used to get an approximate correction for $\partial i_t/\partial \delta_e$, which was presented in reference 5 for a 25 percent chord elevator, to account for the difference in chord ratios. The values used for C_{h_δ}, $\partial i_t/\partial \delta_e$, and q are presented in table II.

Based on the results of reference 5 it was assumed that C_{h_α} was zero for the calculations. Figure 15 presents the calculated variation with Mach number of the increment in elevator deflection required per 0.10 change in lift coefficient.

The elevator deflection required for trim at zero lift with 0° wing and tail incidence was estimated indirectly from the data of figure 9 of reference 4, which was a plot of the variation of normal-force coefficient with Mach number of an XF-91 rocket model in free flight. These data were used in the calculations rather than the wing flow data because of the uncertainty of the angles of zero lift obtained from the wing flow data. The C_L values obtained from reference 4 are noted in table II. Substituting the missile lift coefficients in expression (1) the values of elevator deflection for trim at zero lift were obtained and the corresponding control forces for an unbalanced elevator were calculated. Since the missile center of gravity was 10 percent ahead of the location used for these calculations, the calculated values of elevator deflection and control force for the $0g$ curves may be on the order of 20 percent low in the high Mach number range. Figure 16 presents the calculated variation with Mach number of elevator deflection and control force for trim at zero lift.

By substituting the increment of lift coefficient required per g in (1) the increment of elevator deflection per g was obtained. This increment of elevator deflection was added to the zero lift value given in figure 16 to obtain a curve of elevator deflection for trim in 1g flight which is also plotted in figure 16. The corresponding elevator control forces with an aerodynamically unbalanced elevator are presented.

Because the data indicate that the airplane is considerably out of trim at a Mach number of 0.65 with the center of gravity at 15 percent $\bar{c}$ and the stabilizer set at 0°, the stick forces and elevator angles were recomputed for an assumed stabilizer incidence of -3°. These data are also shown in figure 16.

Although the variation of elevator angle for trim at zero lift, which was based on the rocket model data (reference 4), indicates relatively small trim changes through the Mach number range, the elevator angle for trim at 1 g shows a large upward variation with increasing Mach numbers above a Mach number of 0.85. This variation is caused primarily by the large increase in stability with increasing Mach numbers. This condition would be felt by the pilot as a powerful "tucking under" tendency, unless the associated control force variation was reduced to a reasonable value by use of a suitable booster mechanism.

Figure 17 presents a plot of elevator stick force per g and elevator deflection per g. These data indicate that with the center of gravity at 15 percent $\bar{c}$, the power of the elevator to maneuver the XF-91 airplane would be very limited at Mach numbers near unity. It is also indicated that about 98 percent of the elevator hinge moment must be supplied by a control booster to obtain satisfactory control forces at Mach numbers near unity.

CONCLUSIONS

The wing-flow tests of the $\frac{1}{40}$-scale XF-91 model led to the following conclusions:

1. The variation of the force and moment coefficients with angle of attack or tail incidence was linear from $M = 0.55$ to $M = 1.10$ through an angle of attack range of $-1°$ to $8°$ and a tail incidence range from $-6°$ to $3°$.

2. The control-fixed stability of the complete configuration for maneuvers at constant velocity increased greatly at Mach numbers above 0.85. The aerodynamic center of the XF-91 model shifted from 25 percent $\bar{c}$ at $M = 0.55$ to 60 percent $\bar{c}$ at $M = 1.05$.

3. The value of the downwash factor $\partial\epsilon/\partial\alpha$ at the tail of the XF-91 model increased from about 0.30 at a Mach number of 0.65 to 0.35 at a Mach number of 0.85 and then decreased until at a Mach number of approximately 0.95, $\partial\epsilon/\partial\alpha$ was equal to approximately zero.

4. The contribution of the tail to the longitudinal stability was essentially constant with increasing Mach number. This resulted from the fact that decreasing tail effectiveness was compensated for by the increasing value of the factor $1 - \frac{\partial\epsilon}{\partial\alpha}$, on which the angle of attack of the tail depends, as the Mach number was increased. The tail produced approximately a 20 percent rearward shift in the location of the aerodynamic center.

The calculated elevator angles and stick forces in the transonic range, with no aerodynamic balance assumed, indicated large increases in the elevator angle per g and force per g in maneuvers above a Mach number of 0.85. Large increases were also shown in up elevator deflection and pull force to maintain level flight above a Mach number of 0.85.

Langley Aeronautical Laboratory
  National Advisory Committee for Aeronautics
    Langley Field, Va.

            Harold L. Crane
          Aeronautical Research Scientist

           Arnold R. Beckhardt
         Aeronautical Research Scientist

Approved: Melvin N. Gough
    Chief of Flight Research Division

MMC

REFERENCES

1. Weiberg, James, and Anderson, Warren E.: Wind-Tunnel Investigation
   of the Low-Speed Characteristics of a 1/8-Scale Model of the
   Republic XF-91 Airplane with a Vee and a Conventional Tail.
   Addendum - Characteristics with a Revised Conventional Tail and
   Drooped Wing Tips. NACA RM No. SA8A02, U. S. Air Force, 1948.

2. Ross, Don H.: Wind Tunnel Tests on Republic Aviation Corporation
   Model MX-809. M.I.T. Wind Tunnel Rep. No. 736, June 1946.

3. Ross, Don H.: Wind Tunnel Tests on Republic Aviation Corporation
   Model MX-809, Second Series. M.I.T. Wind Tunnel Rep. No. 745,
   Oct. 1946.

4. Alexander, Sidney R.: Flight Investigation to Determine the Aero-
   dynamic Characteristics of Rocket-Powered Models Representative
   of a Fighter-Type Airplane Configuration Incorporating an Inverse-
   Taper Wing and a Vee Tail. NACA RM No. L8G29, 1948.

5. Johnson, Harold I.: Measurements of Aerodynamic Characteristics of
   a 35° Sweptback NACA 65-009 Airfoil Model with $\frac{1}{4}$-Chord Plain Flap
   by the NACA Wing-Flow Method. NACA RM No. L7F13, 1947.

6. Gilruth, R. R., and White, M. D.: Analysis and Prediction of Longi-
   tudinal Stability of Airplanes. NACA Rep. No. 711, 1941.

TABLE I

GEOMETRIC CHARACTERISTICS OF FULL-SCALE AIRPLANE AND $\frac{1}{40}$-SCALE MODEL

	Full scale	Semispan model
Wing:		
Section (normal to 50 percent chord line).	R-4,40-1$_7$10-1.0	R-4,40-1$_7$10-1.0
Thickness (normal to leading edge), percent. . . .	9.1	9.1
Incidence, deg	Variable	0
Twist, deg	0	0
Sweepback at $0.50\bar{c}$, deg . .	40	40
Inverse taper ratio	1:1.626	1:1.626
A	3.07	3.07
$\bar{c}$, ft	10.6	0.265
b, ft	31.34	0.392
S, sq ft	320.0	0.100
Tail:		
Section	R-4,40-.010X	R-4,40-.010X
Dihedral, deg	38	38
Sweepback (plan view) . . .	40	40
b_t (in horizontal plane), ft	16.30	0.206
c_t, ft	3.94	0.0985
S_t, sq ft	80.0	0.025
Fuselage:		
Length, ft	43.3	1.165
Maximum frontal area of half fuselage, sq ft . .	12.99	0.00813
Tail length ($0.25\bar{c}$ to $0.25\bar{c}_t$), ft	16.7	0.417

NACA

TABLE II

PARAMETERS USED IN CALCULATING CONTROL

POSITIONS AND CONTROL FORCES

M	q (lb/sq ft)	C_L (level flight)	$\dfrac{\partial i_t}{\partial \delta}$	$\dfrac{\partial i_t}{\partial \delta}$ (corrected)	C_{h_δ}	C_L (missile)
0.65	288	0.271	0.270	0.292	-0.0094	-0.008
.70	333	.235	.268	.289	-.0095	-.007
.75	381	.205	.265	.286	-.0097	-.001
.80	437	.179	.253	.263	-.0100	.002
.85	489	.160	.240	.259	-.0103	.006
.90	550	.142	.225	.243	-.0111	.020
.95	615	.127	.210	.227	-.0119	.019
1.00	682	.115	.170	.184	-.0135	-.009
1.05	753	.104	.175	.189	-.0169	-.016

NACA
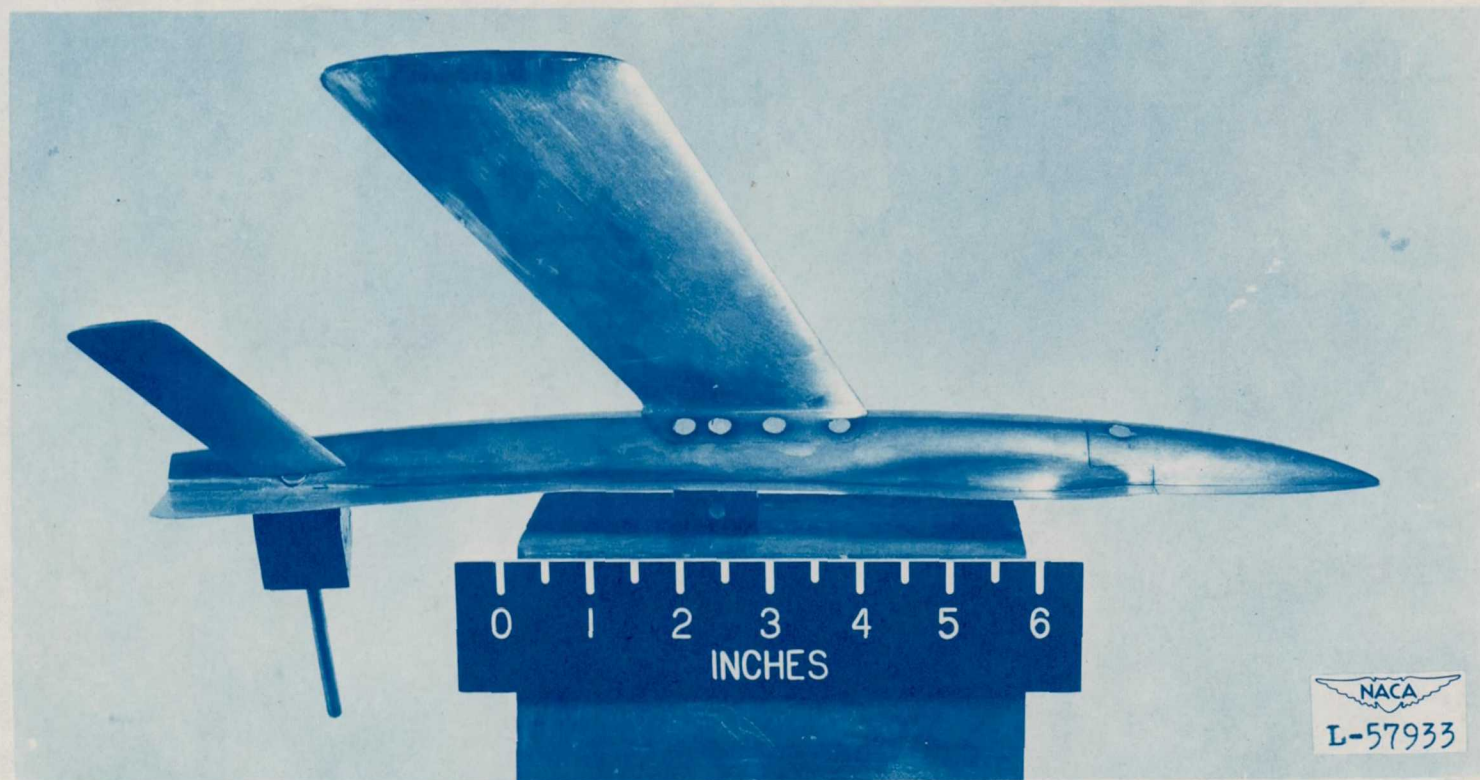
(a) Top view of wing-flow model.

Figure 1.- Photographs of $\frac{1}{40}$-scale wing-flow model of the XF-91 airplane and test apparatus.
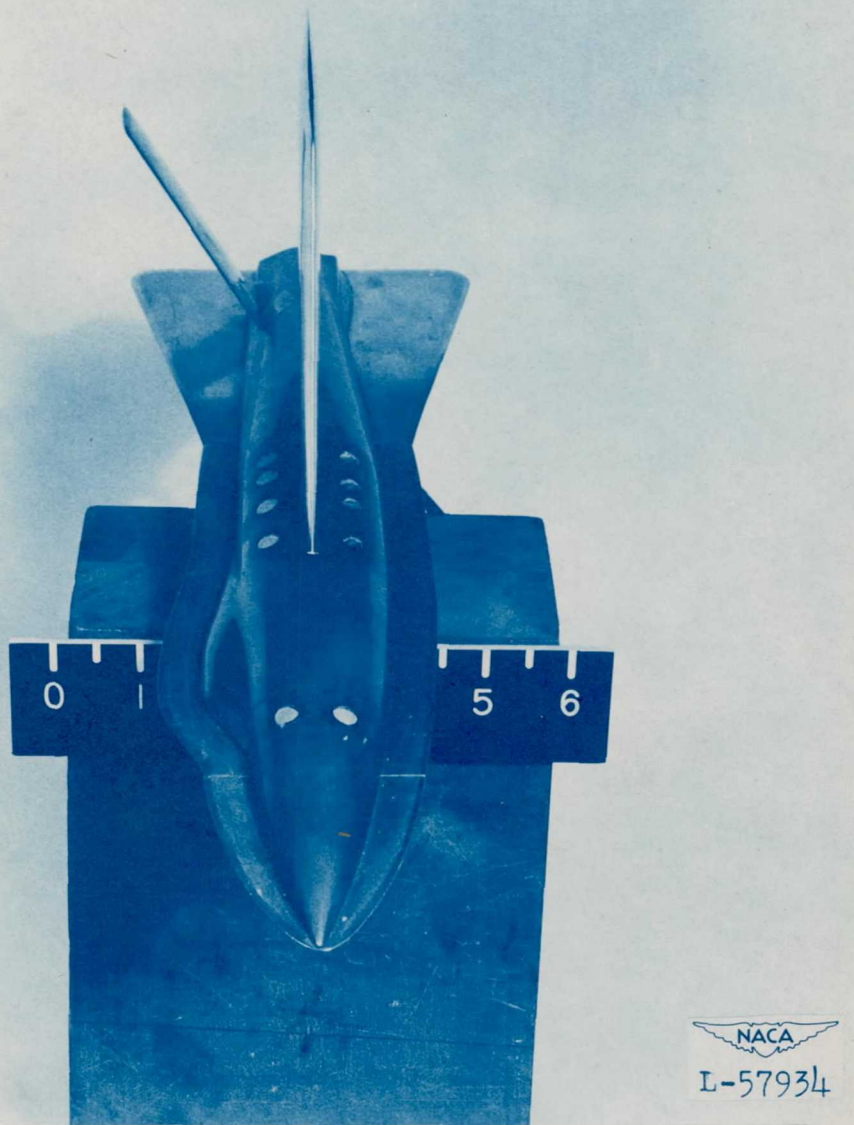
(b) Three-quarter front view of wing-flow model.

Figure 1.- Continued.

2668
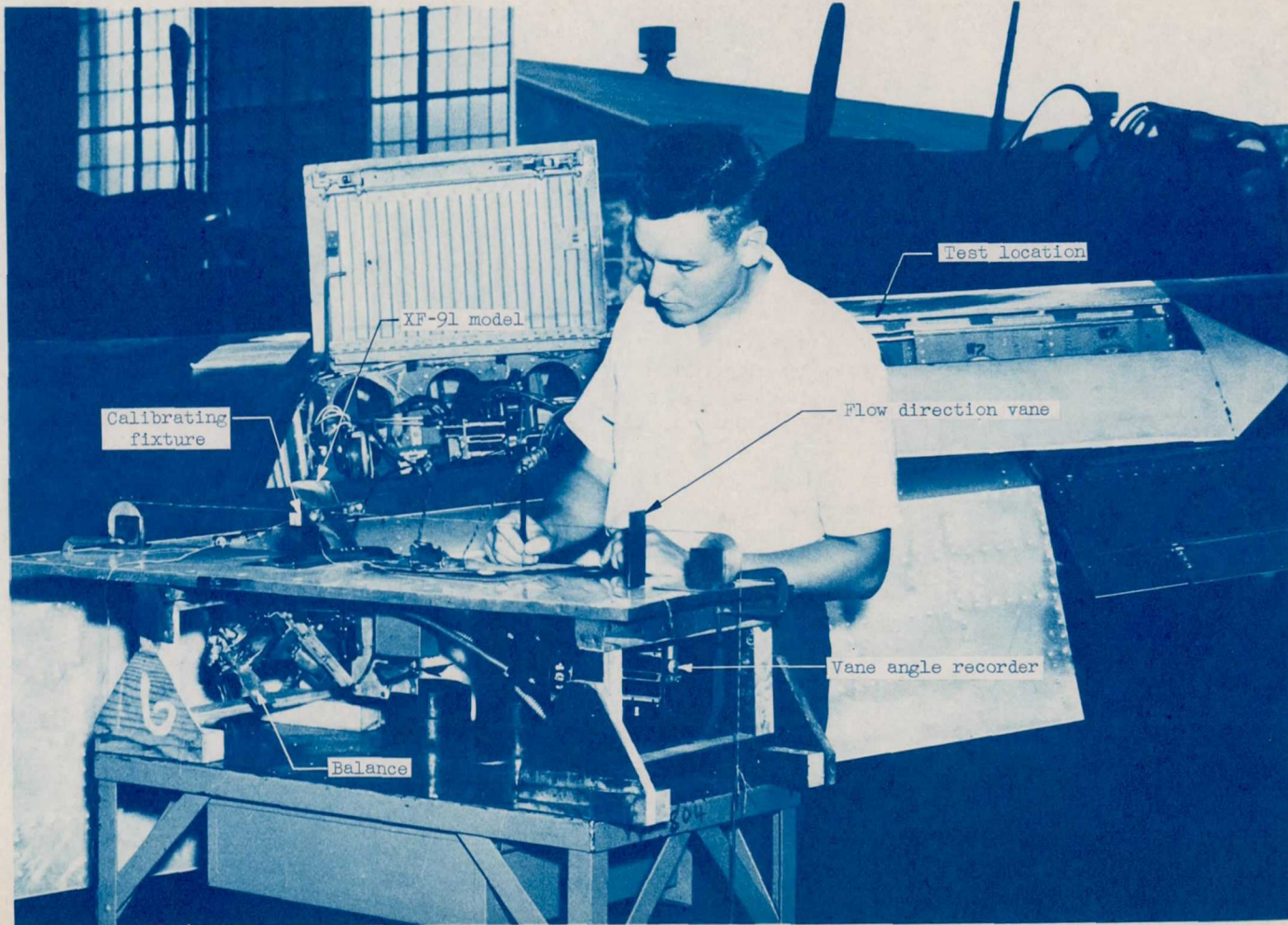
(c) General view of test apparatus.

Figure 1.- Concluded.

L-54032
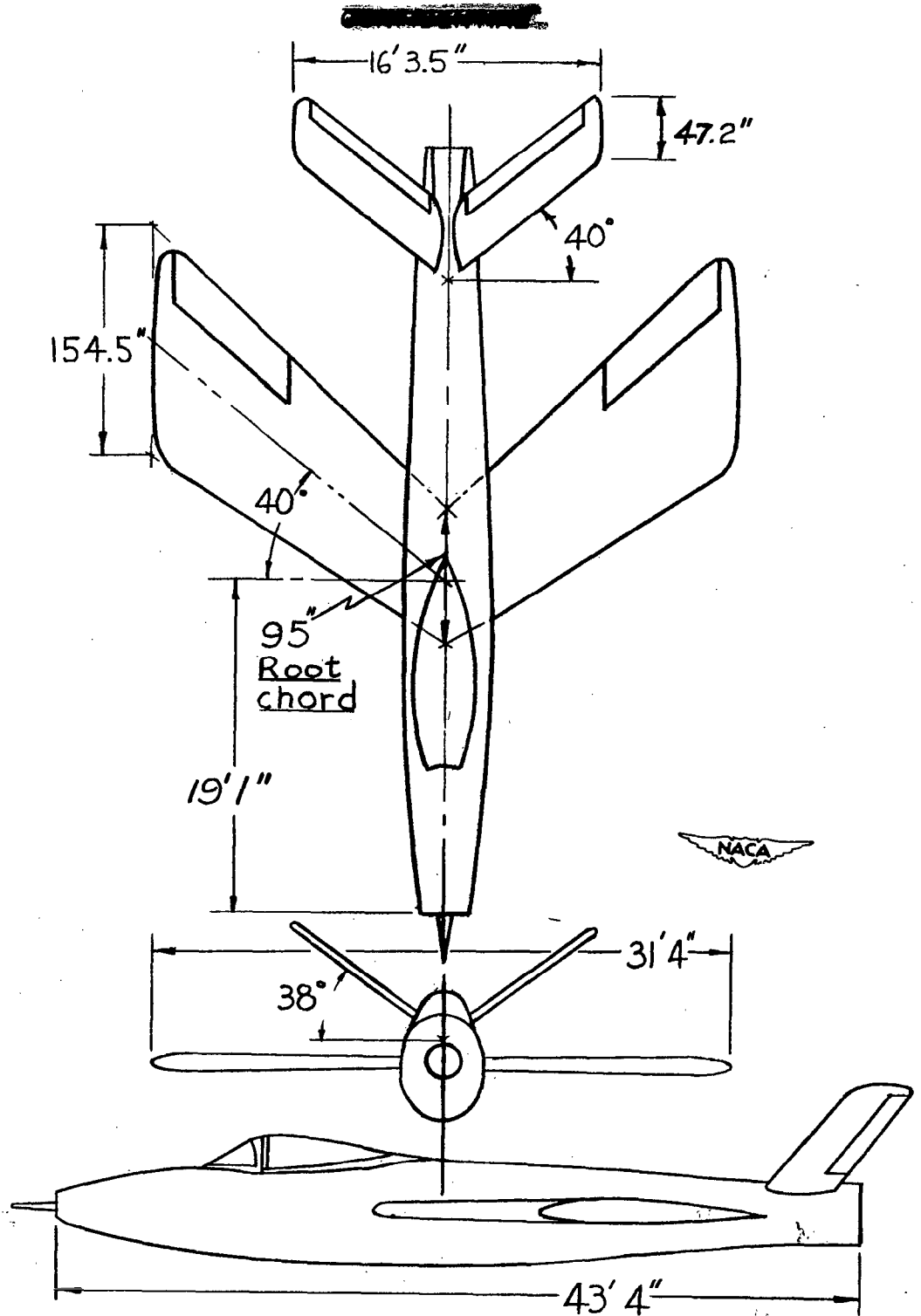
Figure 2.- Three-view drawing of XF-91 airplane showing
principal dimensions.

Wing section   R-4,40-1,10-1.0
Tail section   R-4,40-.010 x

|← 14.0 →|
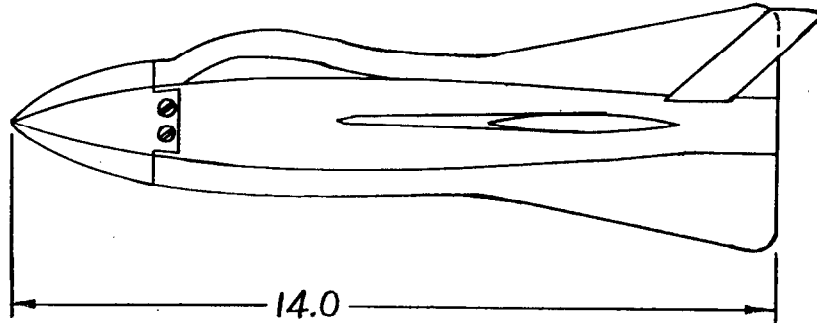
All dimensions in inches

$S = 14.40$ sq in.
$S_t = 3.60$ sq in.
$\bar{C} = 3.18$ in.
$\bar{C}_t = 1.18$ in.

℄ of balance
℄ at 15% $\bar{c}$
50% C
55% c.

|← 3.86 →|

℄ rotation

4.70

40°

1.18

40°

2.44

38°

.40

Break in fuselage
for wing mounting

Airplane
℄

.50

5.0

156.0 R.

.08 Gap

4.75

Wing door

End plate

.032

℄ of rotation

NACA
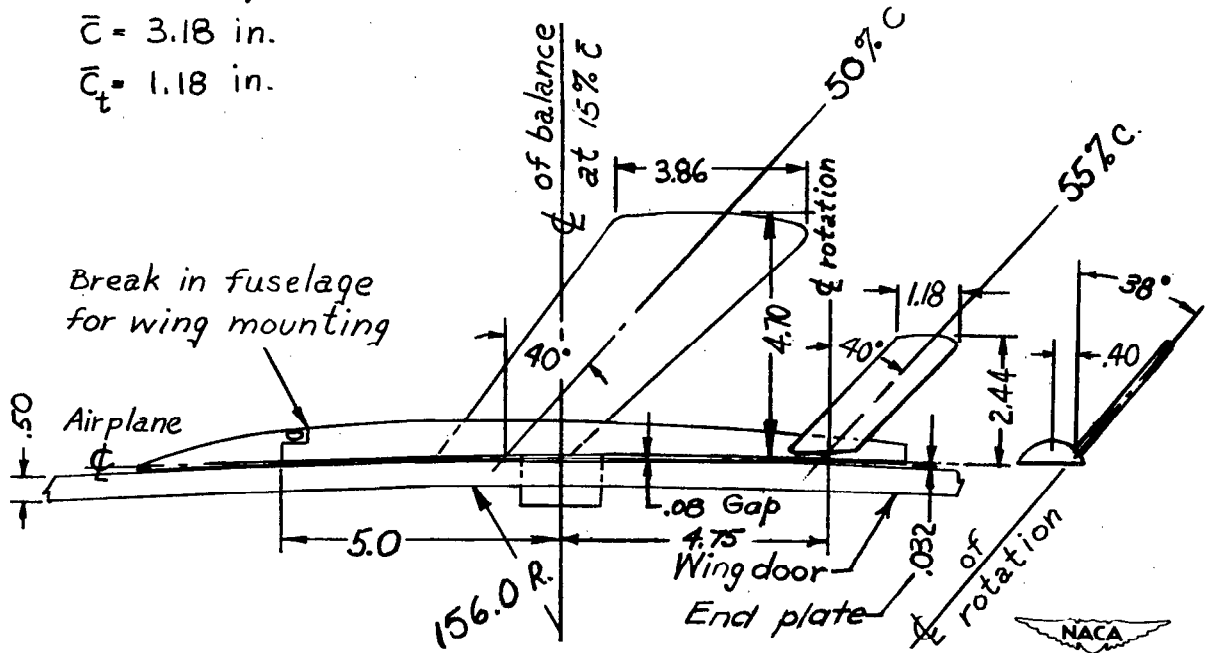
Figure 3.- Drawing of $\frac{1}{40}$-scale XF-91 wing-flow model showing
principal dimensions.
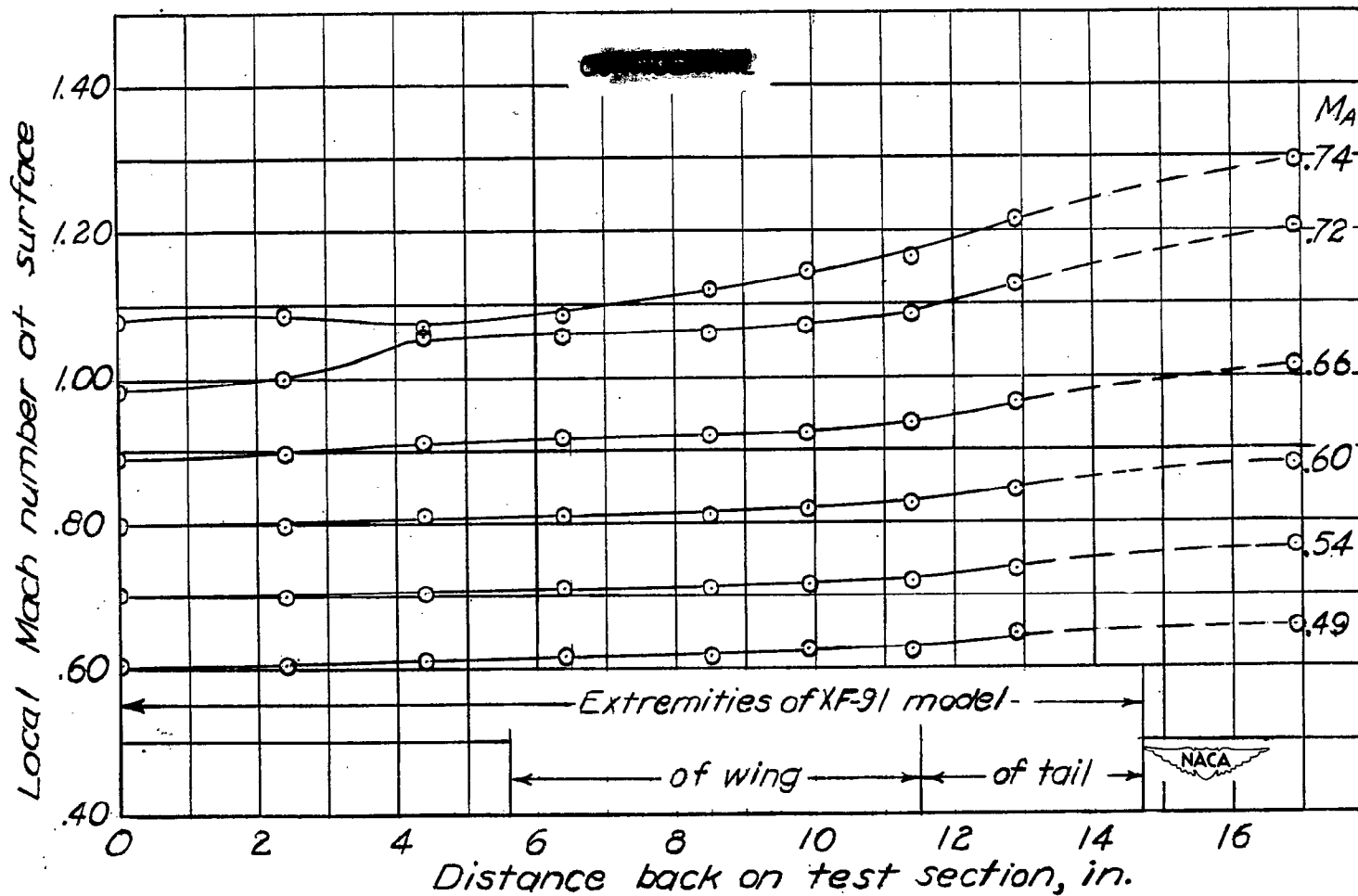
(a) Typical chordwise gradient.

Figure 4.- Local Mach number gradients at test section for various values of airplane Mach number M_A.
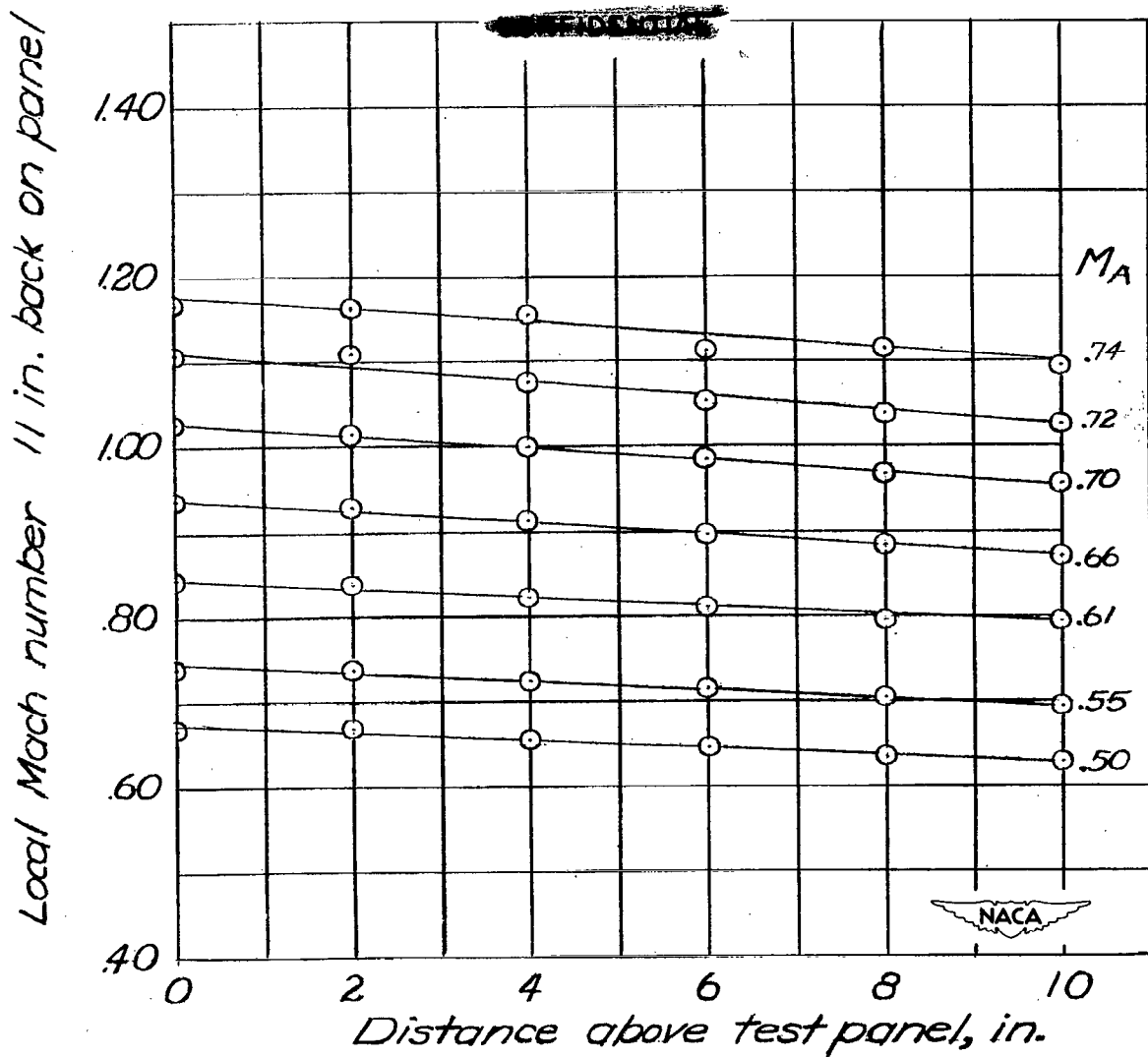
(b) Typical vertical gradient.

Figure 4.- Concluded.
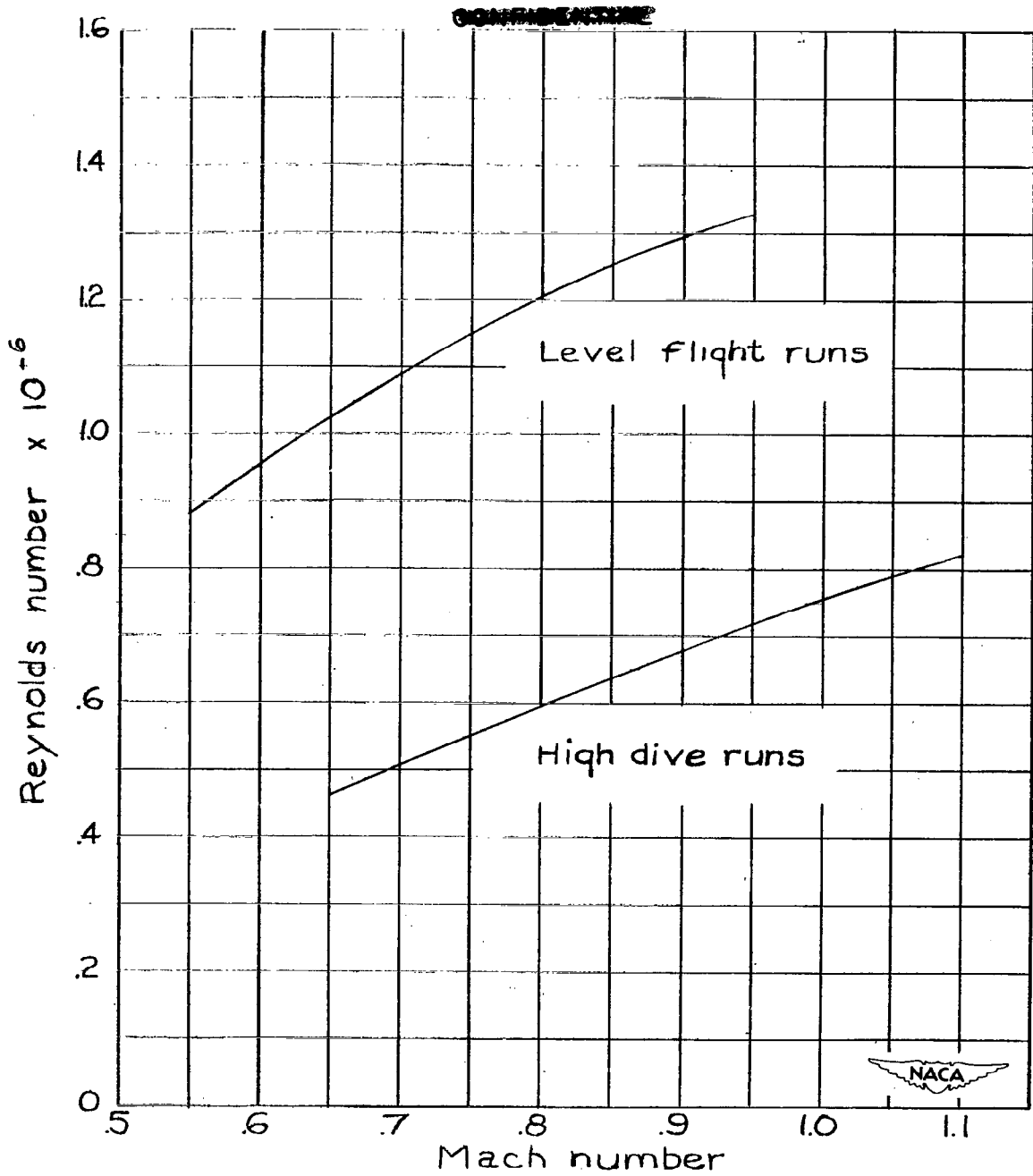
Figure 5.- Variation of Reynolds number with Mach number for XF-91 model based on mean aerodynamic chord of wing.

2668 6

Model angle of attack

Hinge moment

Lift

Pitching moment

$\frac{1}{100}$ Second

$\frac{1}{10}$ Sec

25

26

Rolling moment

Elapsed time, seconds

Sensitivity

Reference line

NACA

Figure 6.- Typical data as first obtained from galvanometer with tail fixed and model oscillating; $\frac{1}{40}$-scale XF-91 model.
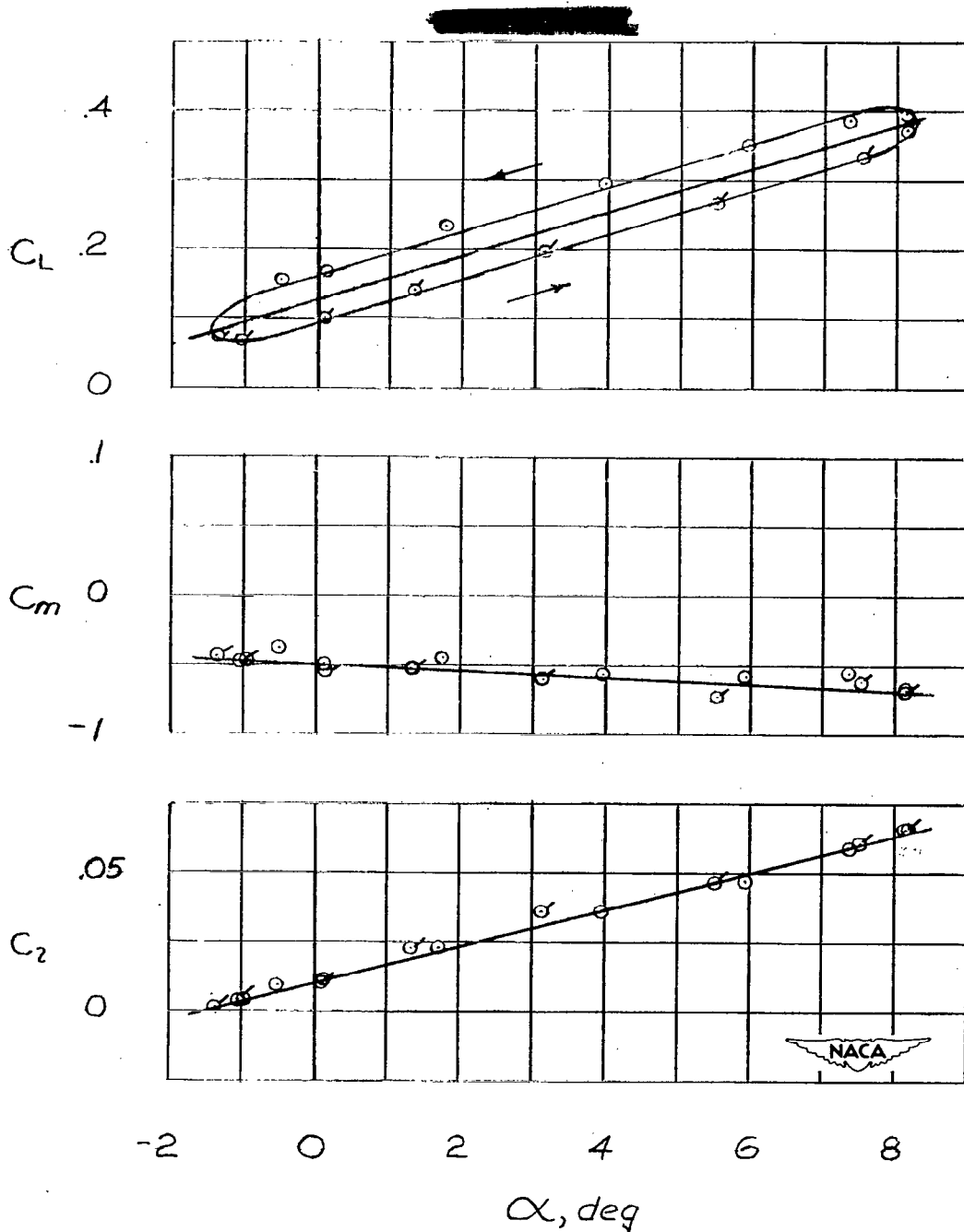
(a) Tail off. M = 1.00; R = 1,300,000.

Figure 7.- Typical examples of wing-flow data as they were first plotted for the $\frac{1}{40}$-scale model XF-91.
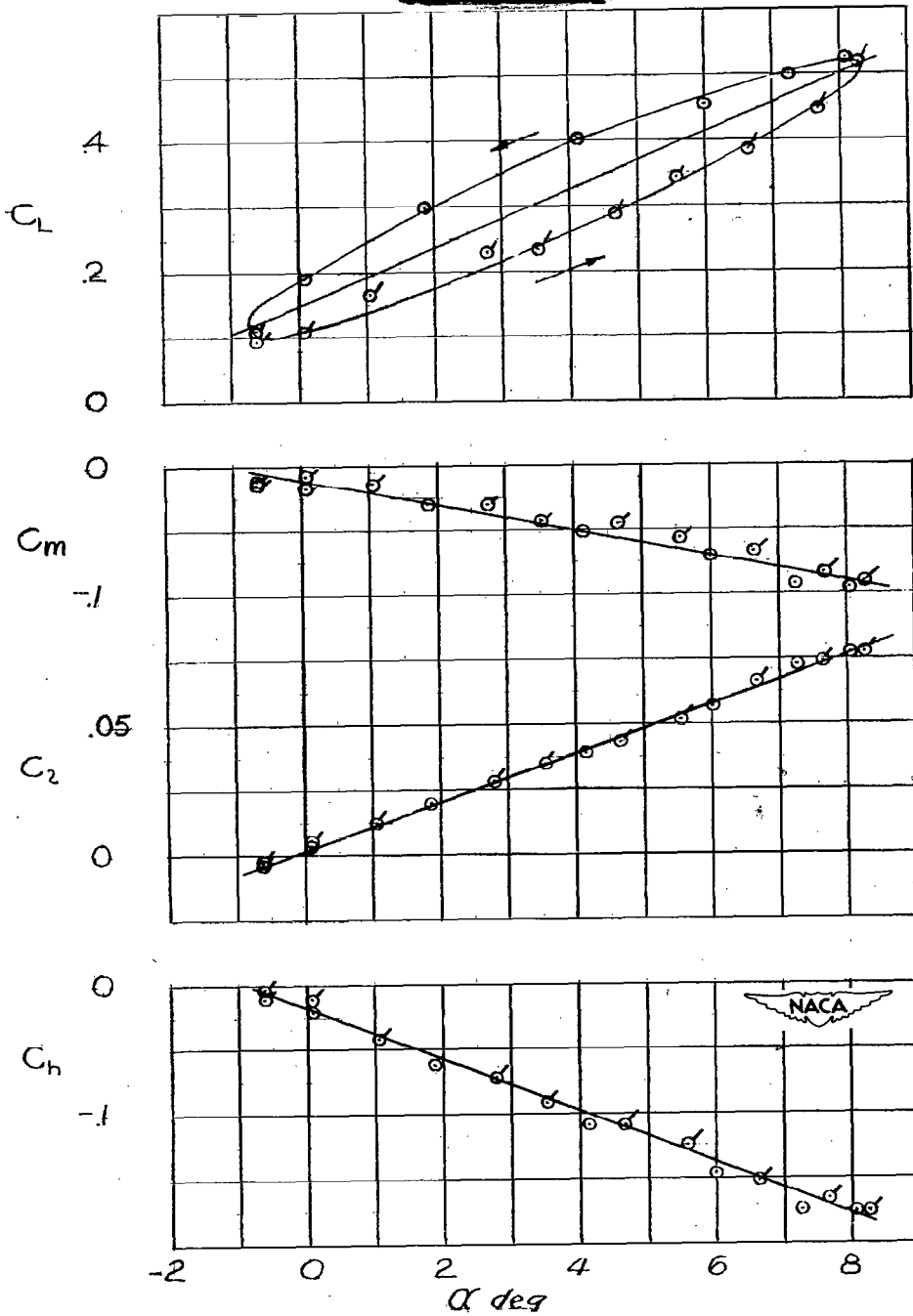
(b) Tail on and fixed.   M = 1.05; R $\cong$ 790,000.

Figure 7.- Continued.
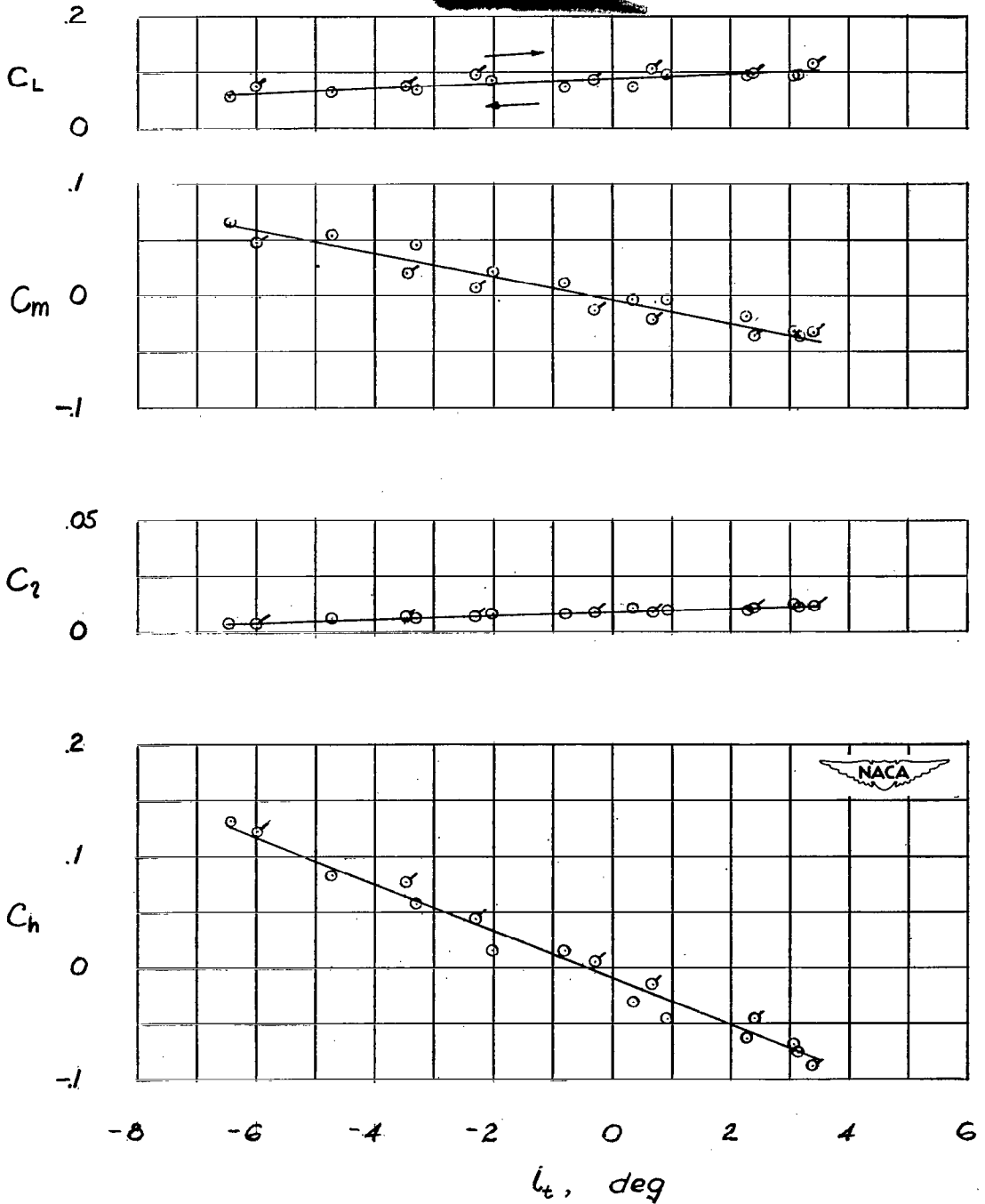
(c) Tail oscillating with model fixed. M = 1.00; R $\cong$ 760,000.

Figure 7.- Concluded.
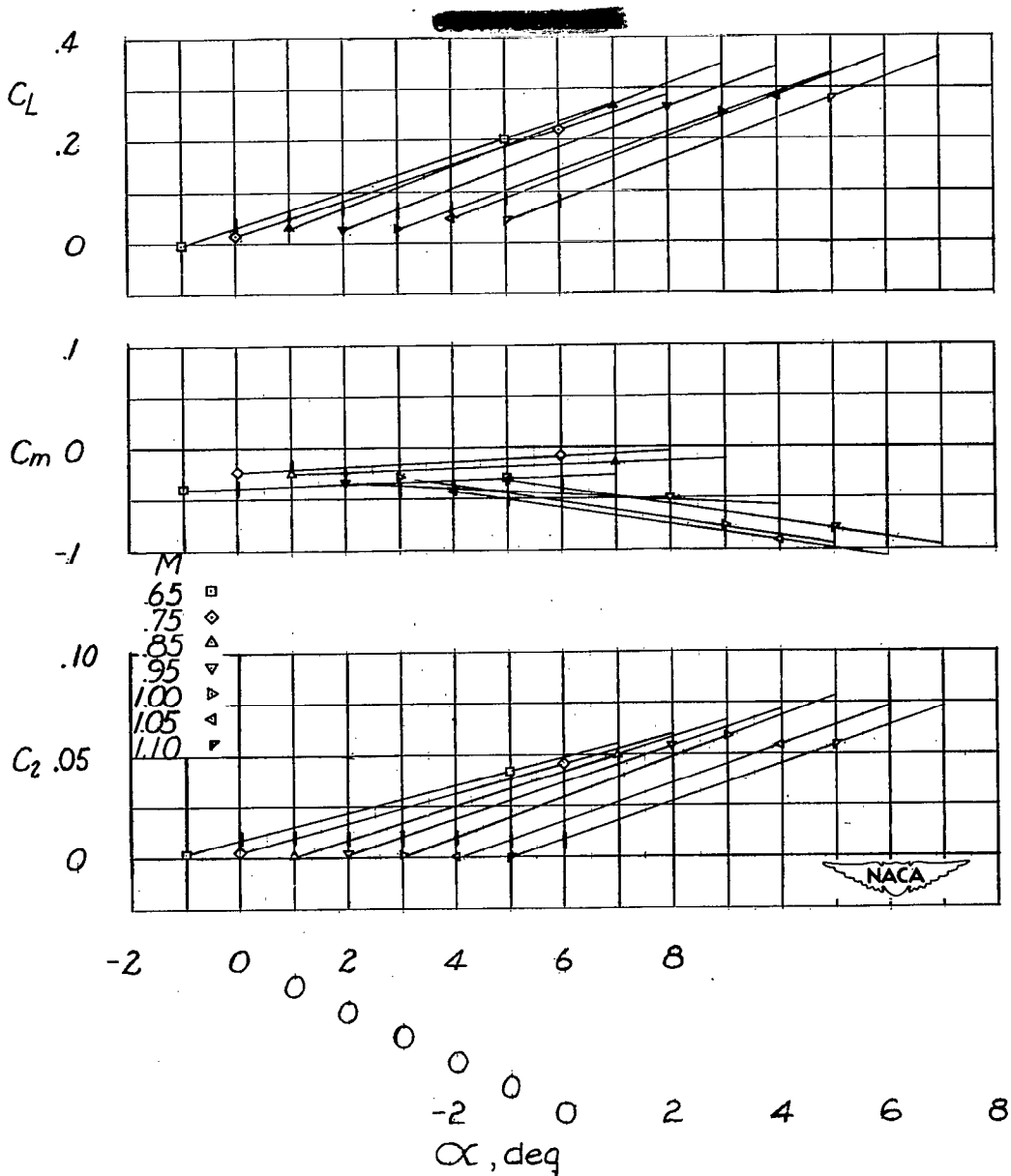
(a) Reynolds number from 460,000 to 820,000.

Figure 8.- Variation of the coefficients of lift, pitching moment, and rolling moment with angle of attack, at Mach numbers throughout the test range for the XF-91 model with tail removed. Note shift in abscissa zero for different Mach numbers. Symbols used for identification purposes only.
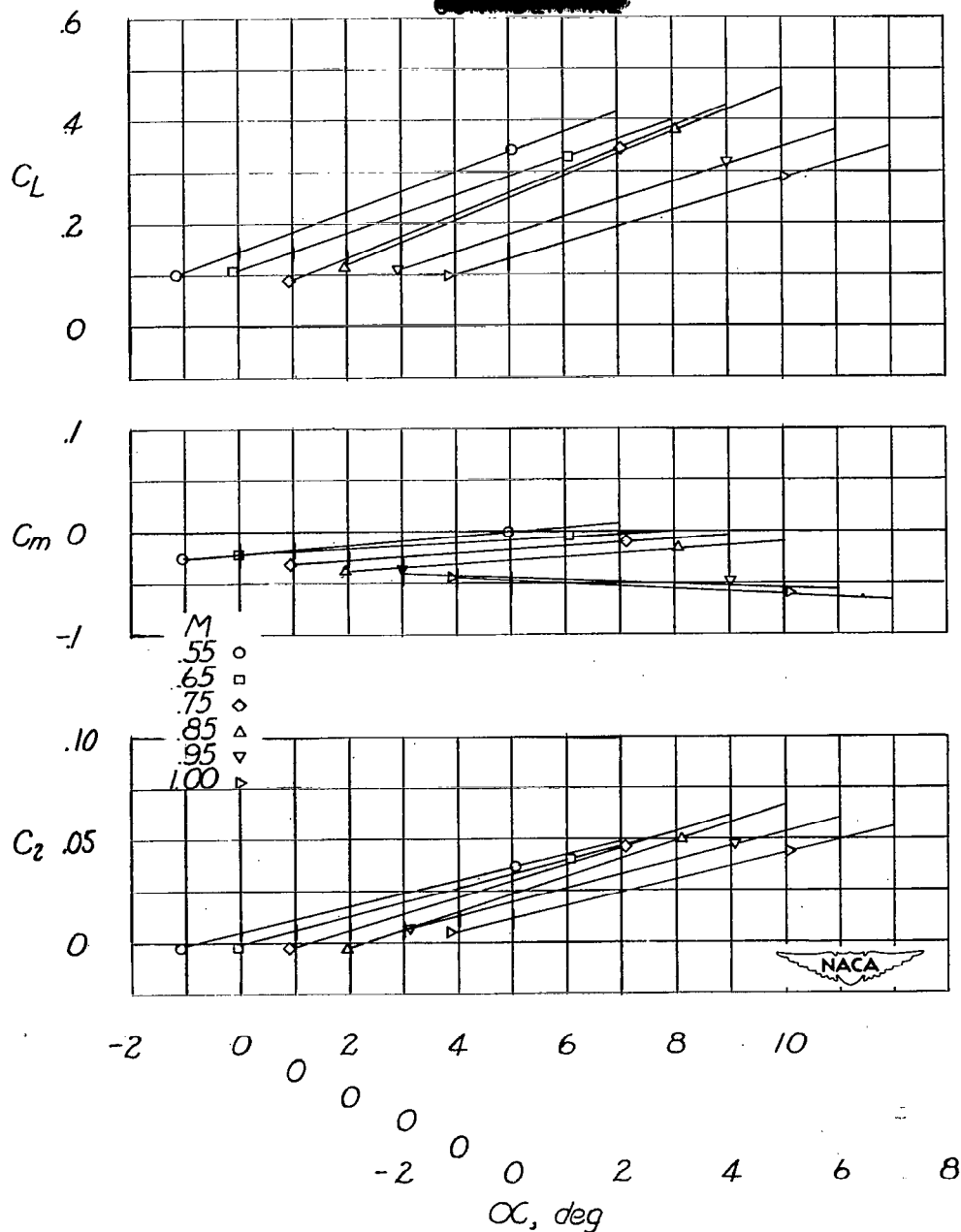
(b) Reynolds number from 800,000 to 1,350,000.

Figure 8.- Concluded.
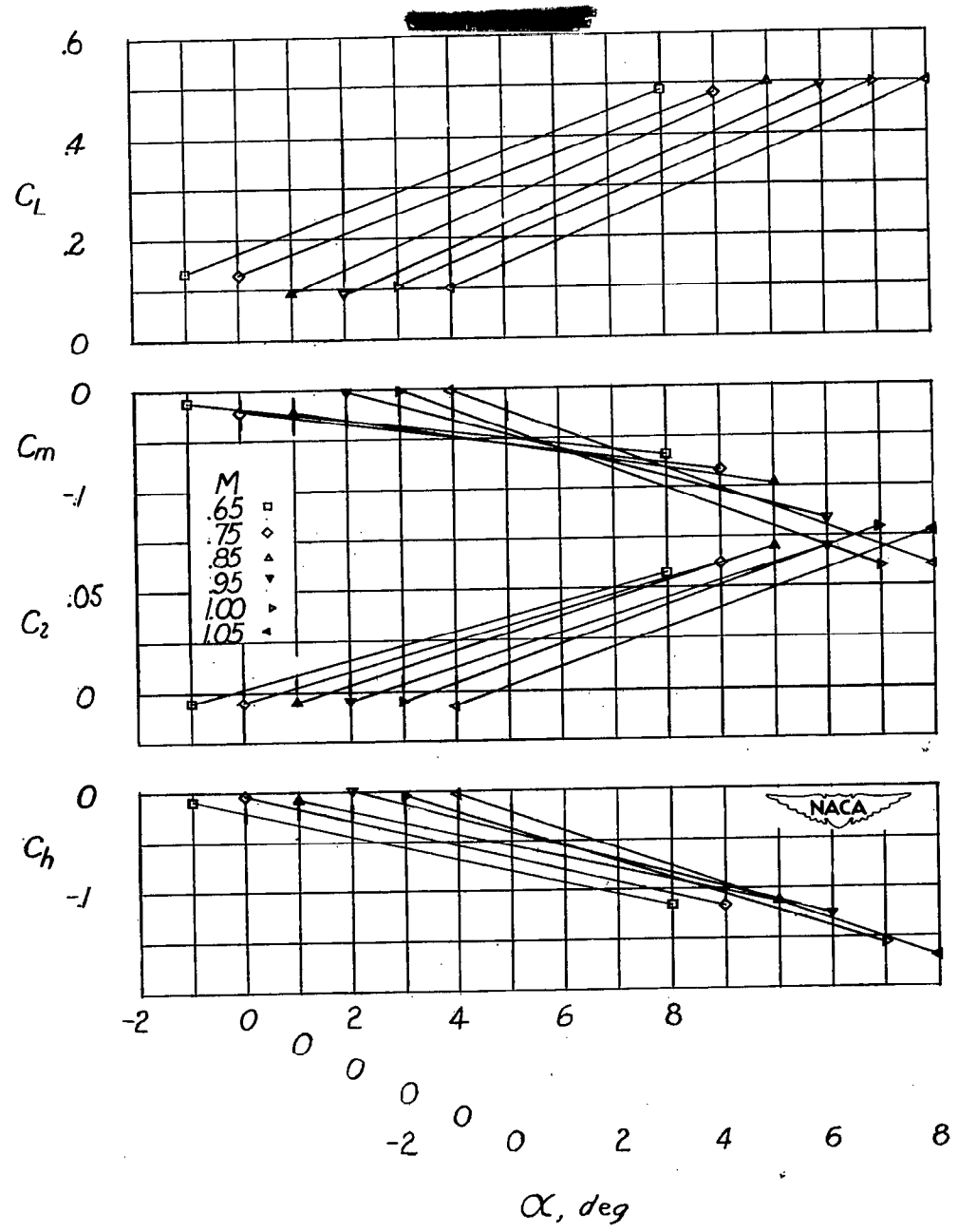
(a) Reynolds number from 460,000 to 790,000.

Figure 9.- Variation of the coefficients of lift, pitching moment,
rolling moment, and hinge moment with angle of attack at Mach
numbers throughout the test range for the XF-91 model with tail
at -1.1°.
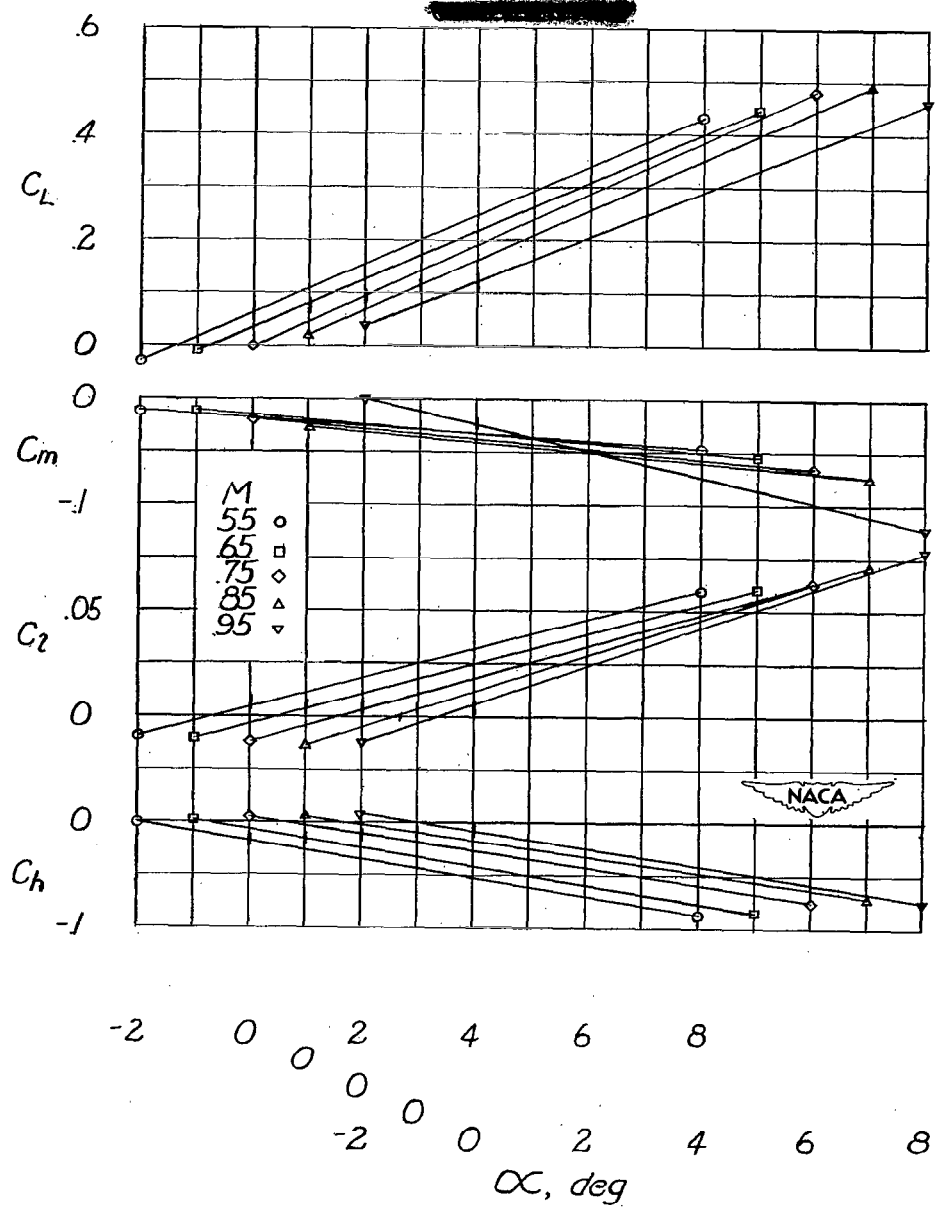
(b) Reynolds numbers from 880,000 to 1,325,000.

Figure 9.- Concluded.
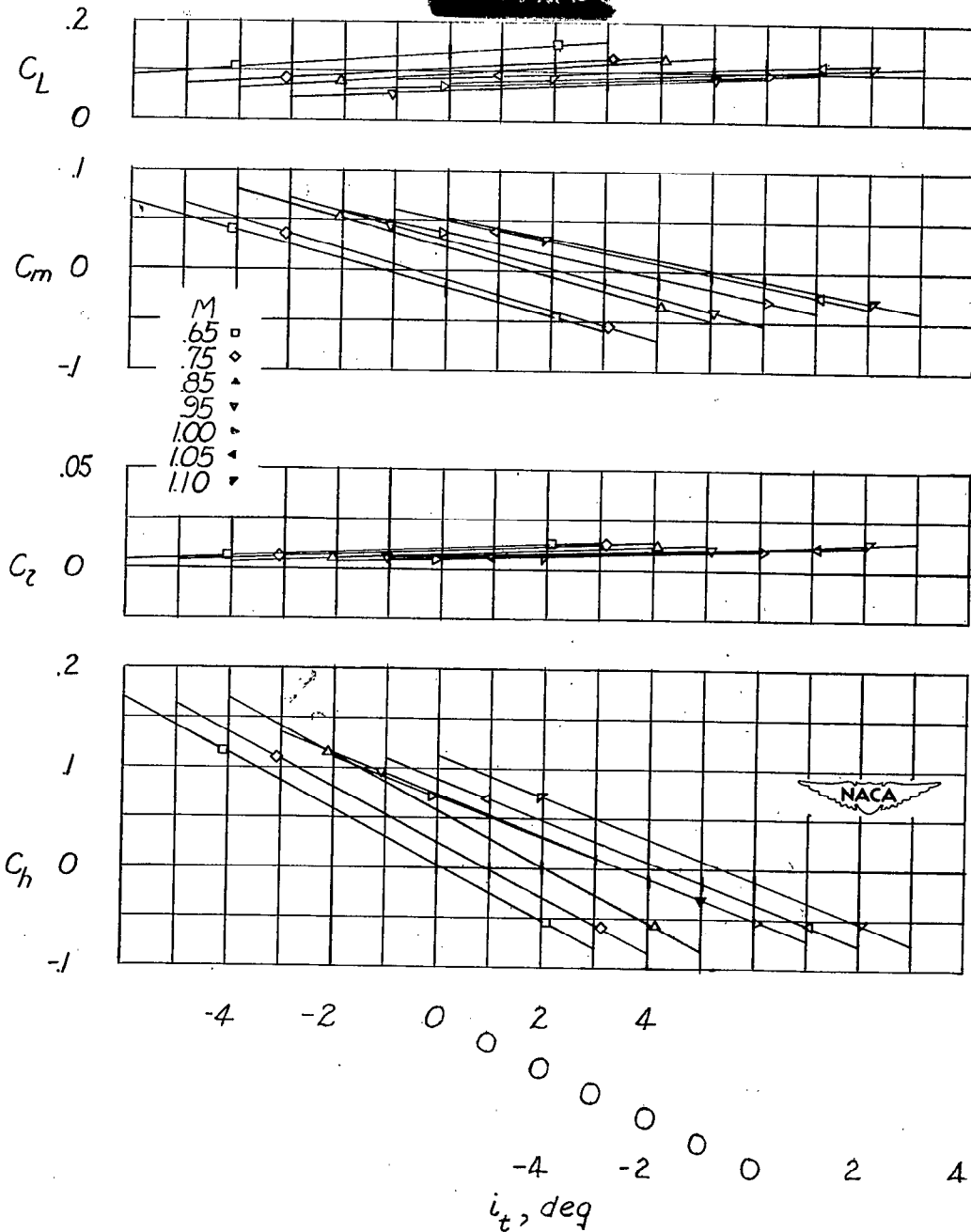
(a) Reynolds numbers from 460,000 to 820,000.

Figure 10.- Variation of the coefficients of lift, pitching moment, rolling moment, and hinge moment with tail incidence at Mach numbers throughout the test range for the XF-91 model.
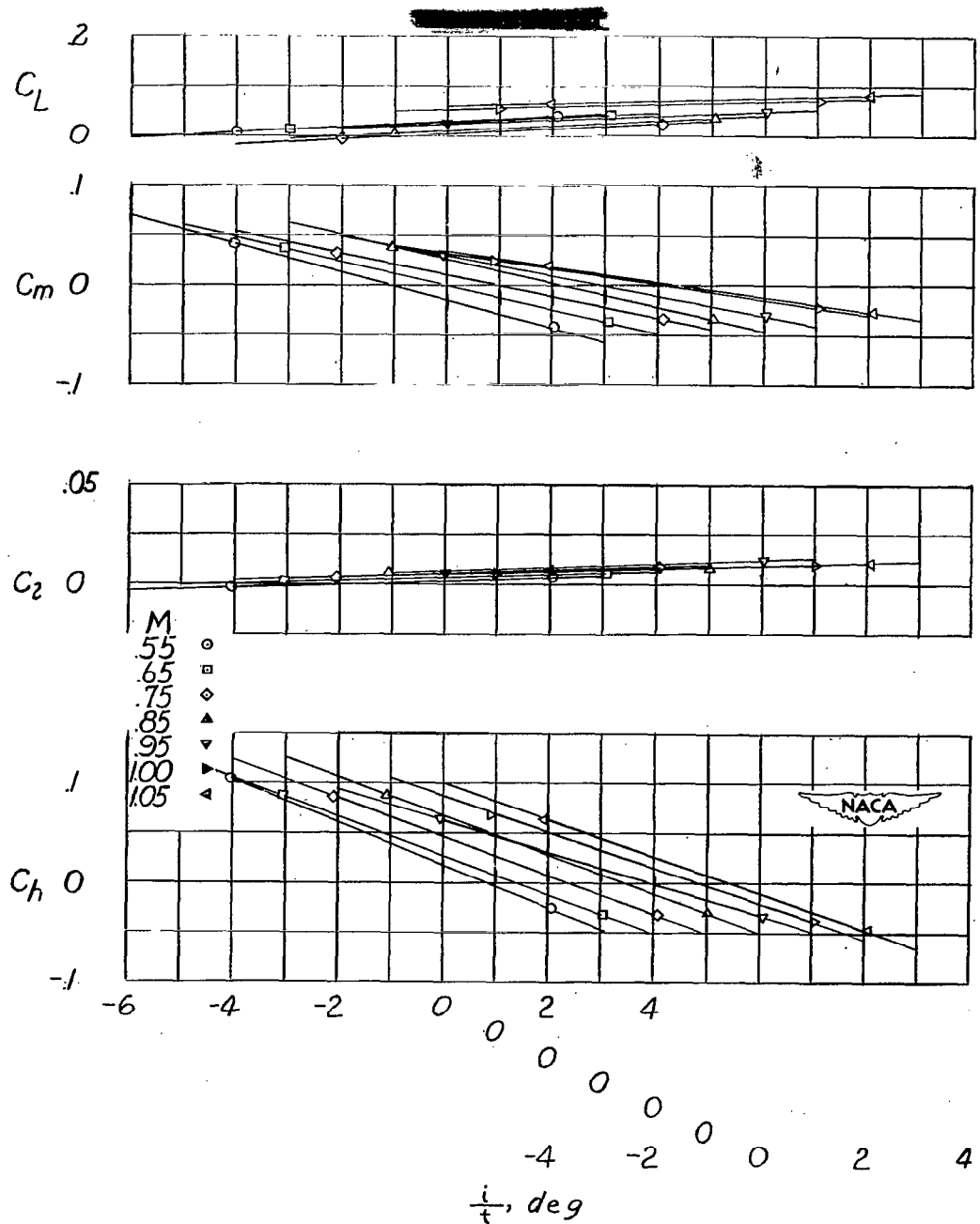
(b) Reynolds numbers from 880,000 to 1,375,000.

Figure 10.- Concluded.
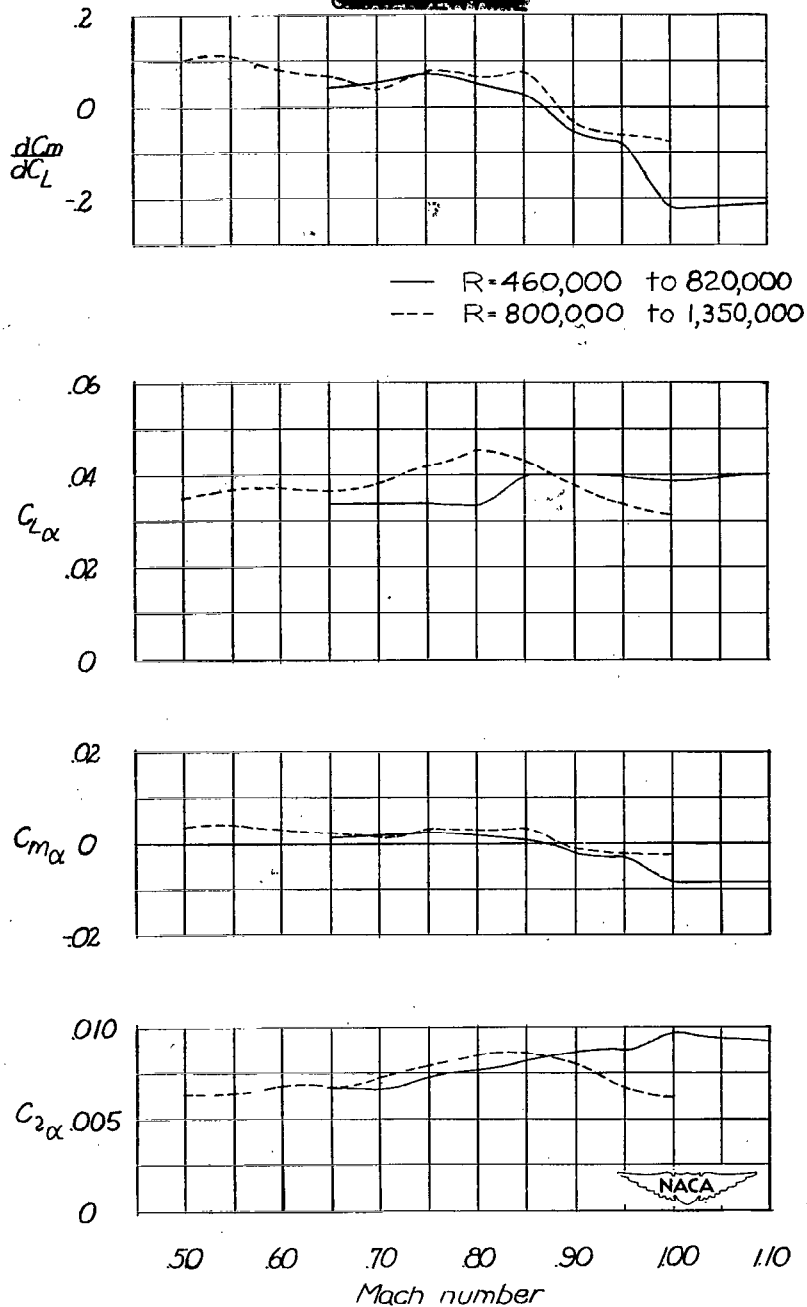
Figure 11.- Variation of $\dfrac{dC_m}{dC_L}$, C_{L_α}, C_{m_α}, and C_{l_α} with Mach number for two Reynolds number ranges for the $\dfrac{1}{40}$-scale XF-91 model with the tail off. Moment reference axis at 15 percent $\bar{c}$.
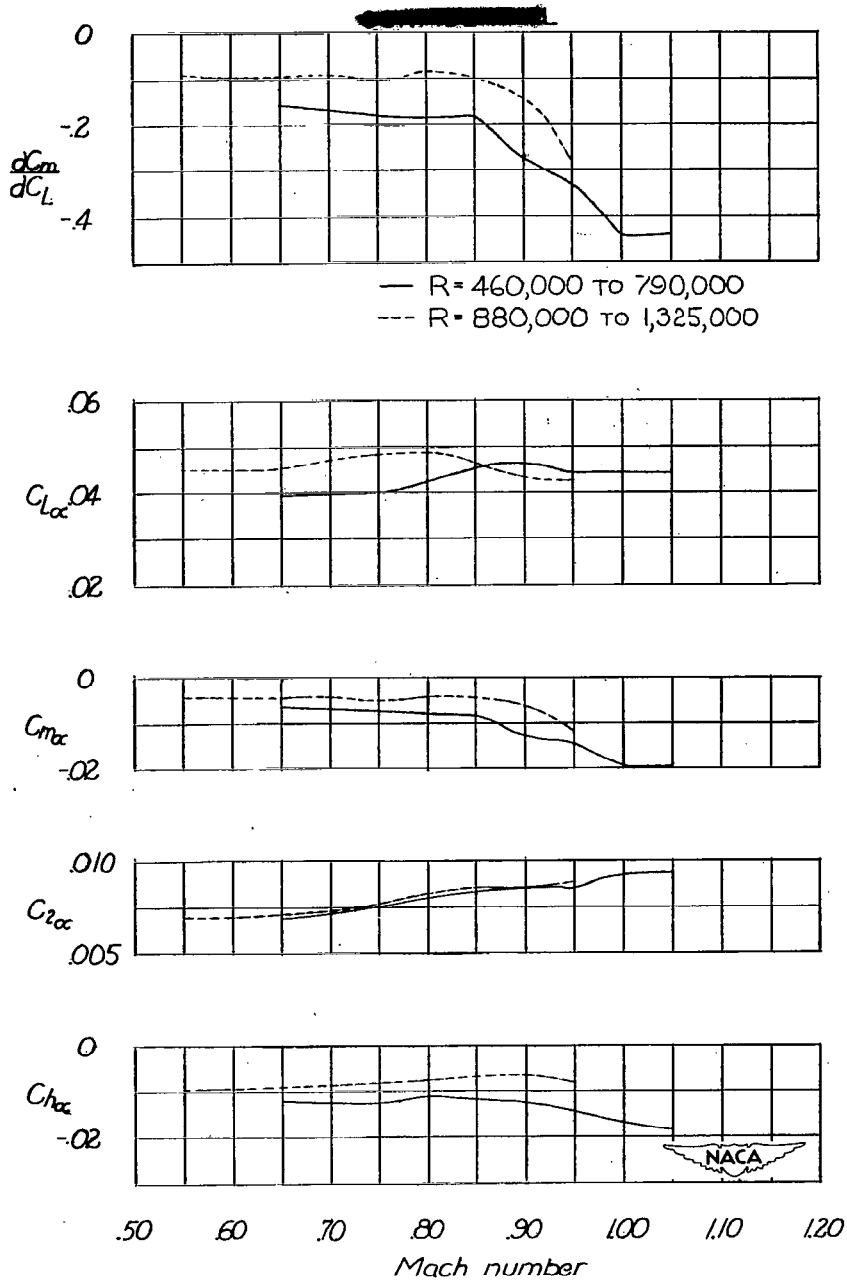
Figure 12.- Variation of $\dfrac{dC_m}{dC_L}$, C_{L_α}, C_{m_α}, C_{l_α}, and C_{h_α} with Mach number for two Reynolds number ranges for the $\dfrac{1}{40}$-scale XF-91 model. Moment reference axis at 15 percent $\bar{c}$.
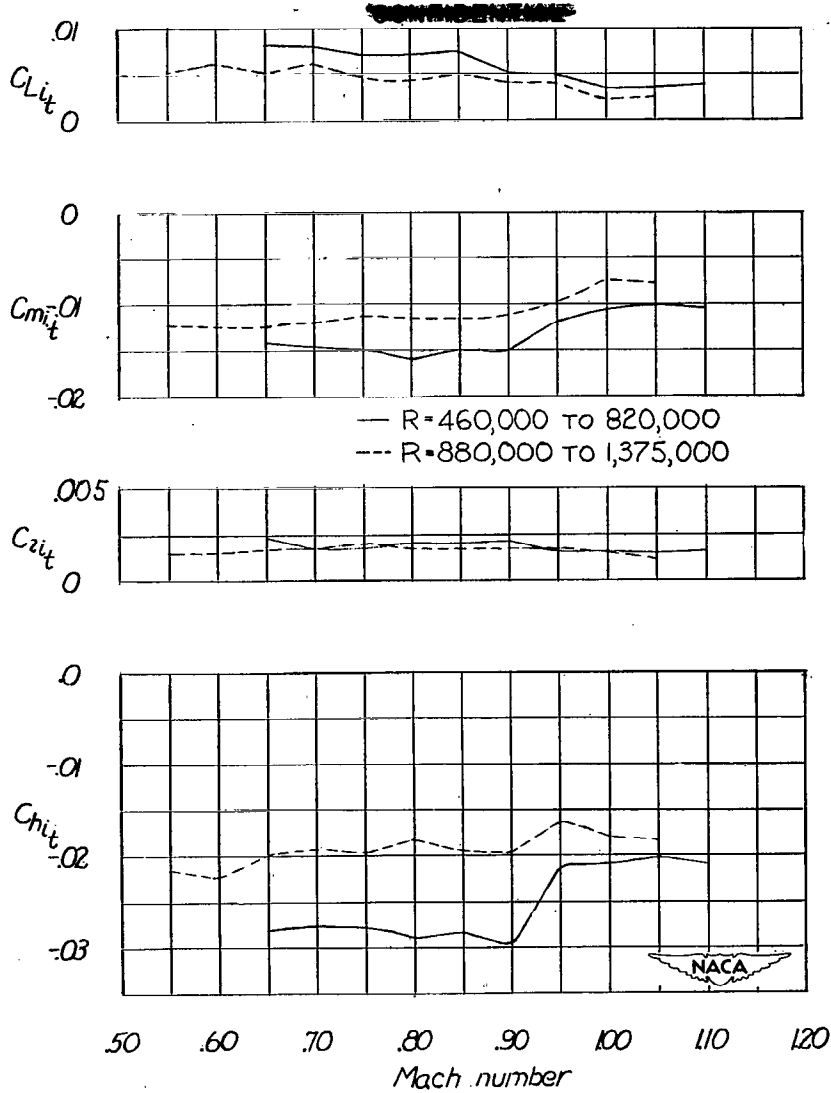
Figure 13.- Variation of $C_{L_{i_t}}$, $C_{m_{i_t}}$, $C_{l_{i_t}}$, and $C_{h_{i_t}}$ with Mach number for two Reynolds number ranges for the $\frac{1}{40}$-scale XF-91 model.
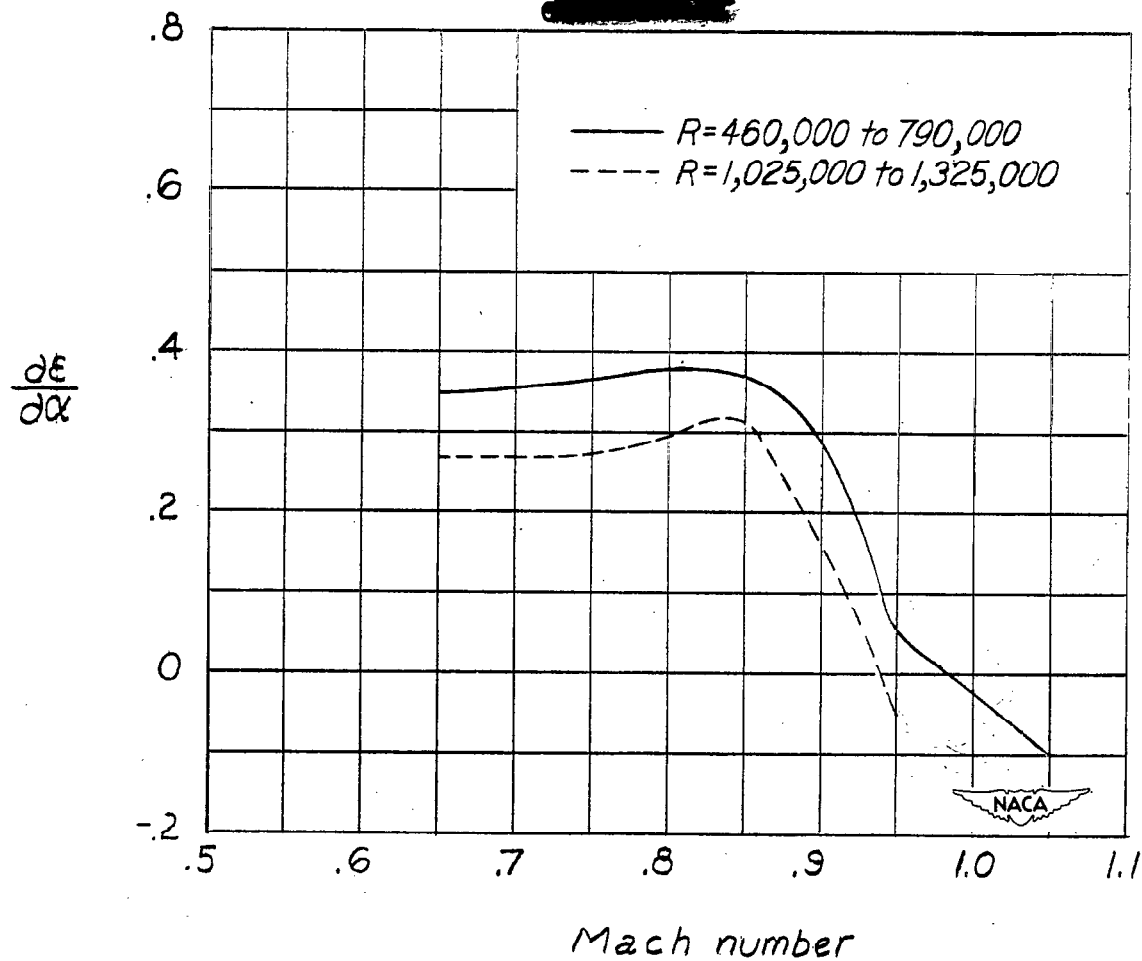
Figure 14.- Variation of the downwash factor $\dfrac{d\epsilon}{d\alpha}$ with Mach number for the flow at the tail of the $\dfrac{1}{40}$-scale XF-91 model at small angles of attack.
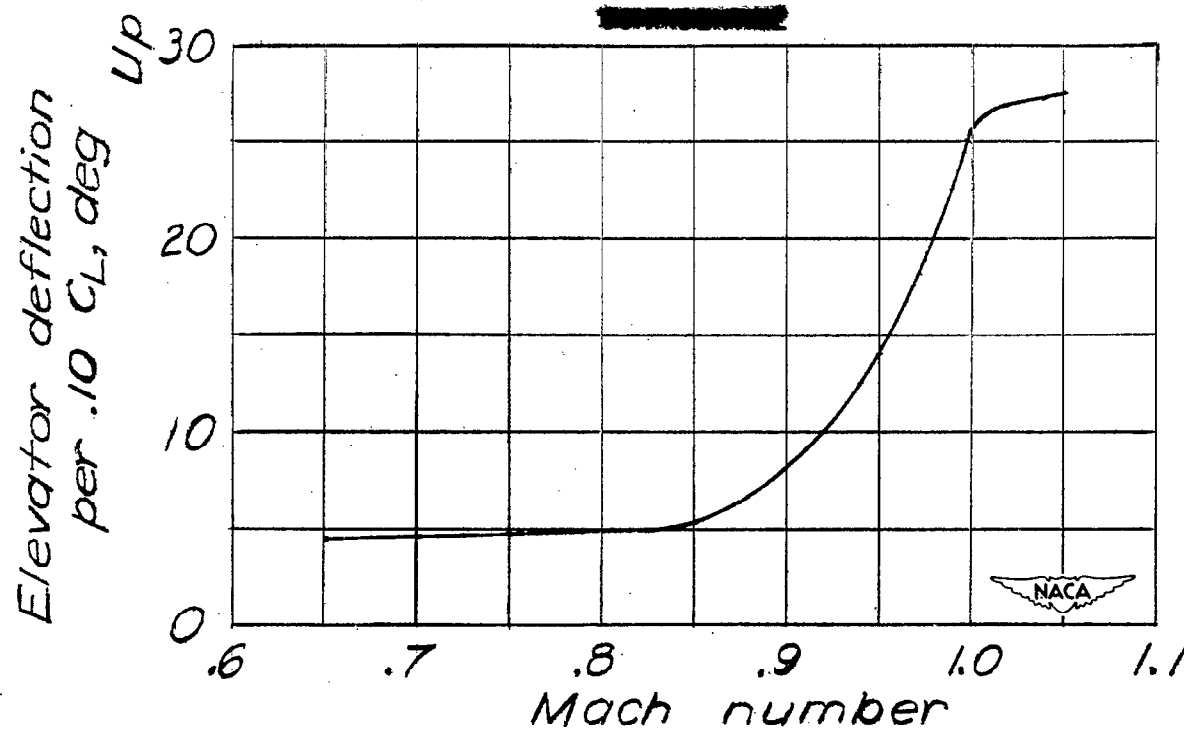
Figure 15.- Calculated elevator deflection per $0.10C_L$ for XF-91 airplane with center of gravity at 15 percent $\bar{c}$.
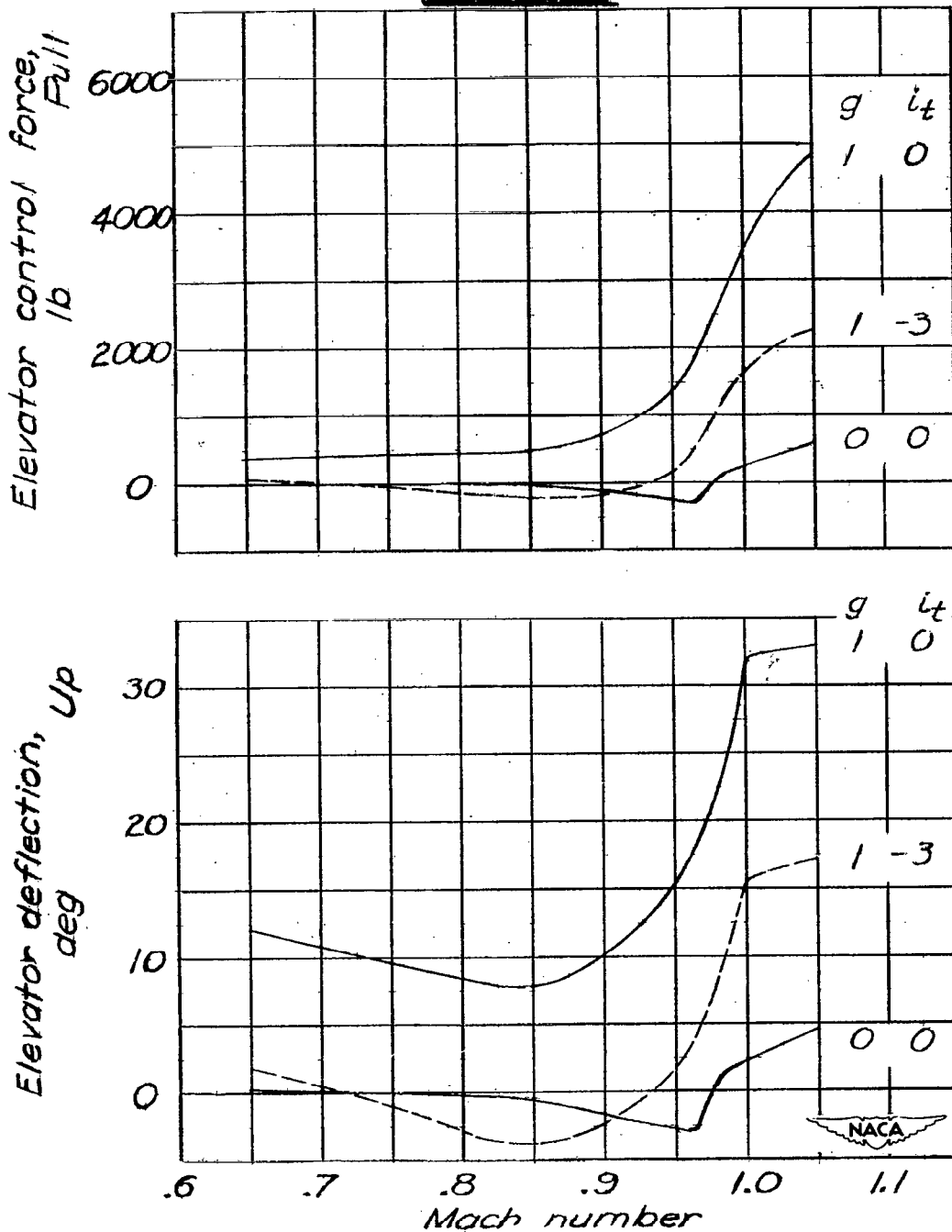
Figure 16.- Calculated elevator deflection and control force for trim at zero lift and in level flight for the XF-91 airplane with the center of gravity at 15 percent $\bar{c}$; altitude 20,000 feet.
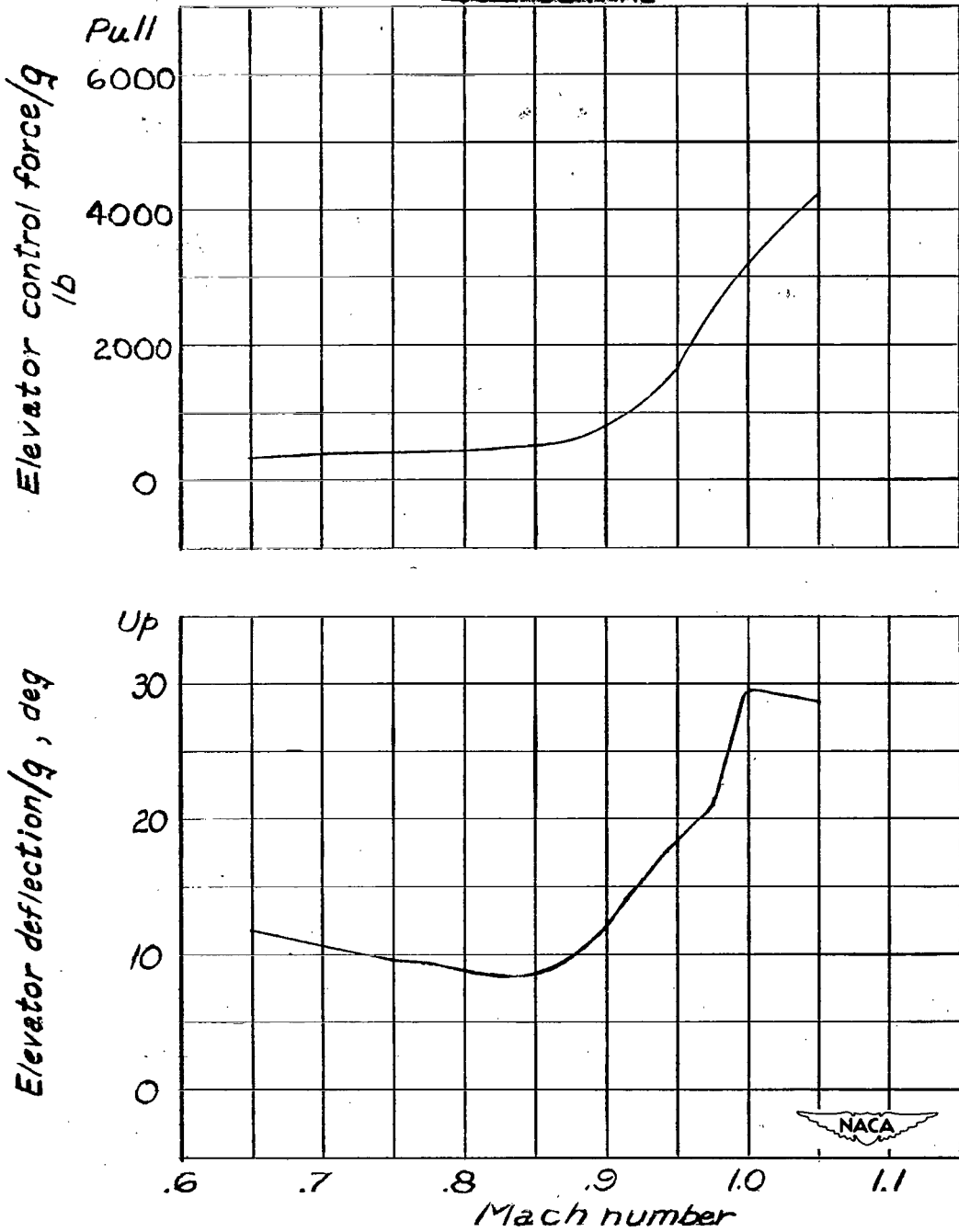
Figure 17.- Calculated values of elevator deflection per g and elevator control force per g for the XF-91 airplane with the center of gravity at 15 percent $\bar{c}$; altitude 20,000 feet.